

TIMING PROPERTIES OF RECENTLY DISCOVERED SOFT GAMMA
REPEATERS

A THESIS SUBMITTED TO
THE GRADUATE SCHOOL OF NATURAL AND APPLIED SCIENCES
OF
MIDDLE EAST TECHNICAL UNIVERSITY

BY

MUHAMMED MİRAC SERİM

IN PARTIAL FULFILLMENT OF THE REQUIREMENTS
FOR
THE DEGREE OF MASTER OF SCIENCE
IN
PHYSICS

SEPTEMBER 2012

Approval of the thesis:

**TIMING PROPERTIES OF RECENTLY DISCOVERED SOFT GAMMA
REPEATERS**

submitted by **MUHAMMED MİRAC SERİM** in partial fulfillment of the requirements for the degree of **Master of Science in Physics Department, Middle East Technical University** by,

Prof. Dr. Canan Özgen _____
Dean, Graduate School of **Natural and Applied Sciences**

Prof. Dr. Mehmet T. Zeyrek _____
Head of Department, **Physics**

Prof. Dr. Altan Baykal _____
Supervisor, **Physics Department, METU**

Assoc. Prof. Dr. Sıtkı Çağdaş İnam _____
Co-supervisor, **Electrical and Electronics Engineering Department, Başkent University**

Examining Committee Members:

Prof. Dr. Sacit Özdemir _____
Astronomy and Space Sciences Dept., Ankara University

Prof. Dr. Altan Baykal _____
Physics Department, METU

Assoc. Prof. Dr. Sıtkı Çağdaş İnam _____
Electrical and Electronics Engineering Dept., Başkent Uni.

Prof. Dr. Ümit Kızılođlu _____
Physics Department, METU

Assist. Prof. Dr. Sinan Kaan Yerli _____
Physics Department, METU

Date: _____

I hereby declare that all information in this document has been obtained and presented in accordance with academic rules and ethical conduct. I also declare that, as required by these rules and conduct, I have fully cited and referenced all material and results that are not original to this work.

Name, Last Name: MUHAMMED MİRAC SERİM

Signature :

ABSTRACT

TIMING PROPERTIES OF RECENTLY DISCOVERED SOFT GAMMA REPEATERS

Serim, Muhammed Miraç

M.Sc., Department of Physics

Supervisor : Prof. Dr. Altan Baykal

Co-Supervisor : Assoc. Prof. Dr. Sıtkı Çağdaş İnam

September 2012, [58](#) pages

In this thesis, the recently discovered Soft Gamma Ray Repeaters SGR J1833-0832, SWIFT J1822.3-1606 and SWIFT J1834.9-0846 are analysed using the archival Swift, RXTE, Chandra and XMM-Newton observations. The period fluctuations and timing noise properties of these sources are investigated. Spectral characteristics and long term frequency evolution of these sources are presented. Investigation for timing noise structure of these magnetars has shown a correlation between first frequency derivative of the spin frequency and torque noise strength.

Keywords: magnetars, soft gamma repeaters, anomalous X-ray pulsars, pulse timing, timing noise

ÖZ

YENİ KEŞFEDİLEN YUMUŞAK GAMA IŞINI TEKRARLAYICILARININ ZAMANLAMA ÖZELLİKLERİ

Serim, Muhammed Miraç

Yüksek Lisans, Fizik Bölümü

Tez Yöneticisi : Prof. Dr. Altan Baykal

Ortak Tez Yöneticisi : Doç. Dr. Sıtkı Çağdaş İnam

Eylül 2012, 58 sayfa

Bu tezde, yeni keşfedilen yumuşak gamma ışını kaynakları SGR J1833-0832, SWIFT J1822.3-1606 ve SWIFT J1834.9-0846 arşivdeki Swift, RXTE, Chandra ve XMM-newton uydularının verileri ile analiz edildi. Kaynakların dönme periyodu deęsimleri ve zamanlama gürültüleri incelendi. Bu çalışmada, kaynakların taysfal özellikleri ve uzun zamanlı dönüş frekansı evrimi sunulmaktadır. Zamanlama gürültüsünün yapısı hakkında yapılan çalışma dönüş frekansının birinci türevi ve zamanlama gürültüsünün kuvveti arasında bir bağıntı olduğunu göstermektedir.

Anahtar Kelimeler: magnetarlar, yumuşak gama ışını tekrarlıyıcıları, anormal X-ışını atarcaları, zamanlama gürültüsü, puls zamanlaması

To my Family

ACKNOWLEDGMENTS

I would like to express my gratitudes to my supervisor Prof. Dr. Altan BAYKAL and co-supervisor Assoc. Prof. Dr. Sıtkı Çağdaş İNAM for their guidance and encouragement during my studies. I am grateful to Assist. Prof. Dr. Sinan Kaan YERLİ for his help and comments. I would like to thank my committee members Prof. Dr. Sacit ÖZDEMİR and Prof. Dr. Ümit KIZILOĞLU.

I also thank my colleague Baha DİNÇEL for his support and helpful comments.

I would like to thank Mehtap Özbey for her help on editing of this thesis. I believe, my colleagues, Burçin İÇDEM, Danjela ÇERRİ, Merve ÇOLAK, Suat DENGİZ, and Şeyda ŞAHİNER deserve thanks for useful discussions.

I acknowlegde the support of TÜBİTAK (The Scientific and Technological Research Council of TURKEY) with the project TBAG-109T748 during this study.

TABLE OF CONTENTS

ABSTRACT	iv
ÖZ	v
ACKNOWLEDGMENTS	vii
TABLE OF CONTENTS	viii
LIST OF TABLES	x
LIST OF FIGURES	xi
CHAPTERS	
1 INTRODUCTION	1
1.1 Soft Gamma Repeaters and Anomalous X-ray Pulsars	2
2 MODELS	5
2.1 Magnetar Model	5
2.2 Fallback Disk Model	7
3 INSTRUMENTS	8
3.1 RXTE	8
3.2 SWIFT	11
3.3 XMM-Newton	12
3.4 CHANDRA	15
4 SOURCES AND OBSERVATIONS	18
4.1 Selected Sources	18
4.2 Observations	21
5 DATA ANALYSIS AND RESULTS	24
5.1 Phase coherent timing	24
5.2 Torque noise	33
5.3 Spectral analysis	34

6	CONCLUSION AND DISCUSSION	45
	BIBLIOGRAPHY	
	APPENDICES	
A	APPENDIX	53

LIST OF TABLES

TABLES

Table 4.1	Journal of RXTE observations. SAT is the satellite observation carried out; N is number of observations; T is total exposure time in ksec.	21
Table 5.1	Timing parameters of SGR J1833–0832	27
Table 5.2	Timing parameters of Swift J1822.3–1606	29
Table 5.3	Spectral parameters of Swift J1834.9–0846	40
Table A.1	Journal of RXTE observations of SWIFT J1822.3-1606 . .	53
Table A.2	Journal of RXTE observations of SGR J1833-0832	54
Table A.3	Journal of RXTE observations of SWIFT J1834.9-0846 . .	55
Table A.4	Journal of SWIFT observations of SWIFT J1822.3-1606 (windowed timing mode)	56
Table A.5	Journal of SWIFT observations for SGR1833-0832 (Photon Counting mode)	57
Table A.6	Journal of other observations.	58

LIST OF FIGURES

FIGURES

Figure 1.1	Pulsar diagram	2
Figure 3.1	Schematics of RXTE Instruments	9
Figure 3.2	Schematics for SWIFT instruments	11
Figure 3.3	Schematics for XMM instruments	13
Figure 3.4	Schematics for Chandra instruments	16
Figure 5.1	Pulse arrival times of SGR J1833–0832	27
Figure 5.2	Timing residuals of SGR J1833–083	28
Figure 5.3	Pulse arrival times of Swift J1822.3-1606	29
Figure 5.4	Pulse profiles of Swift J1834.9–0846	31
Figure 5.5	Pulse arrival times (top panel) and timing residuals (bottom panel) for Swift J1834.9-0846.	32
Figure 5.6	Noise strengths of three SGRs as a function of their pulse frequency derivatives.	34
Figure 5.7	XMM-Newton Spectrum of SGR J1833–0832 with powerlaw model (top panel) and with blackbody model (bottom panel)	36
Figure 5.8	Variation of spectral parameters of SGR J1833–0832 with respect to time using blackbody emission model (top panel) and using power law model (bottom panel).	37
Figure 5.9	Swift spectrum of SWIFT J1822.3–1606 with blackbody model (top panel) and powerlaw model (bottom panel).	38

Figure 5.10	Variation of spectral parameters of SWIFT J1822.3–1606 with respect to time using blackbody emission model (top panel) and using power law model (bottom panel).	39
Figure 5.11	Swift spectrum of Swift J1834.9–0846 with powerlaw model (top panel) and blackbody emission model (bottom panel).	41
Figure 5.12	XMM-Newton spectrum of Swift J1834.9–0846 with blackbody emission model (top panel) and with powerlaw emission model (bottom panel).	42
Figure 5.13	Chandra spectrum of Swift J1834.9–0846 with blackbody emission model (top panel) and powerlaw emission model (bottom panel).	43
Figure 5.14	Pulsed count rate history of Swift J1834.9–0846	44

CHAPTER 1

INTRODUCTION

For a main sequence star, the nuclear fusion within the star causes outward pressure while gravity pushes radially inwards, the balance between these two forces enables the star to maintain its life. As the nuclear fusion chain resumes, heavier elements are formed, if the star is massive and it reaches to iron creation stage, then the internal thermonuclear pressure cannot compensate gravitational force resulting in gravitational collapse of the star causing supernova explosion. If the initial mass of the star is in between 8–25 solar masses, it undergoes supernova explosion which can leave a neutron star as a remnant. That neutron star is called pulsar, if it has strong magnetic field 10^{12} G and it emits beams of light that sweeps through Earth's line of sight, which is seen as a pulse, due to misalignment of its rotational axis and magnetic axis (figure 1). Pulsars are divided into two categories according to the source of their energy: rotation powered pulsars and accretion powered pulsars. For rotation powered pulsars the magnetic dipole braking causes the loss of rotational kinetic energy and that energy is released as magnetic dipole radiation. For the accretion powered pulsars, the gravitational potential energy release of accreted material is thought to be the origin of pulsar's emission.

Soft Gamma Repeaters and Anomalous X-ray pulsars possess observationally distinct properties compared to known accretion-powered and rotation-powered pulsars. They have spin periods in the range of 2–12s with high spin down rates of 10^{-11} s/s (Woods and Thompson 2004), and have softer

¹figure adapted from <http://www.nrao.edu/pr/2003/pulsaremission/>

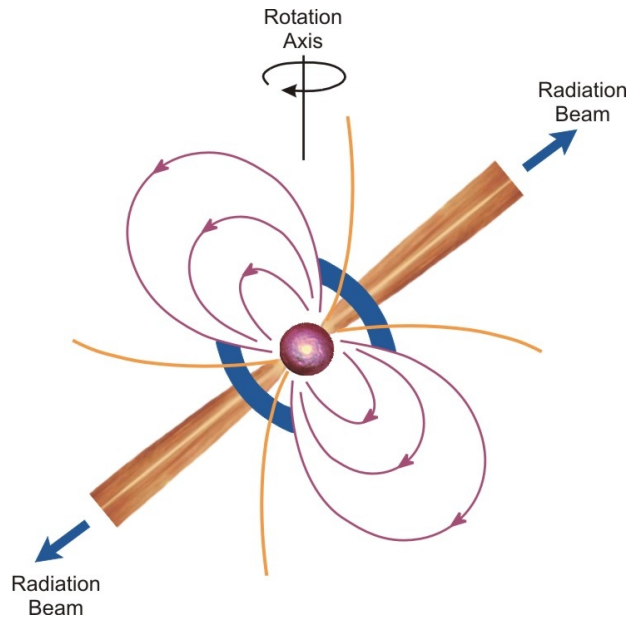


Figure 1.1. Pulsar diagram¹

X-ray spectra compared to accreting X-ray binaries. Their calculated spin down rate corresponds to only few percentage of their observed luminosity. As there is no discovery of any companion or disk, they are thought to be isolated (Mereghetti and Stella 1995). Number of discovered SGRs and AXPs reached up to 23 in total until today (see McGill SGR/AXP Online Catalog²). In order to explain the unique nature of SGRs and AXPs, many emission mechanism models have been proposed however, now there are two widely accepted models; magnetar and fall back disk models.

1.1 Soft Gamma Repeaters and Anomalous X-ray Pulsars

Discovery of the first SGR came in 7 January 1979 (Laros et al. 1986), though at the time scientists were not able to distinguish it from common GRBs. It was the most intense extra-solar burst of gamma rays ever detected on Earth and it was originated from a source located in constellation Sagittarius. Almost two months later, at 5 March 1979, another burst of gamma rays was detected exceeding the scale of gamma ray detectors of on board satellites from a source in Large Magellanic Cloud (Evans et al.

²<http://www.physics.mcgill.ca/pulsar/magnetar/main.html>

1979). The source is associated with supernova remnant N49 (Mazets et al. 1979). The burst initiated with hard gamma ray flare lasting 0.2 seconds and it was followed by a spectrally softer 8 second pulsations with two peaks per cycle as the intensity slowly decays. The following day, March the 6th, another burst came from the same location lasting 1.5 seconds. In the following month, two other bursts were detected from the same source each lasting around 0.2s . These events made scientists think that the source was not a GRB because no GRB has been seen to repeat from the same source.

In 1981, Fahlman and Gregory (1981b) using Einstein X-ray observatory discovered a source in the center of the supernova remnant CTB 109, labeled as 1E 2259+586. It possesses 7 seconds pulsations per cycle, and the Optical/IR observations showed no evidence of massive companion. Even though finding an accreting system in a supernova remnant would be unusual, it was still initially classified as low mass X-ray binary (Fahlman and Gregory 1983), in fact, it was the first AXP ever discovered. Several years after the discovery of 1E 2259+586, another X ray source 1E 1048.1-5937 with 6.44s pulsations was discovered (Seward et al. 1986). Israel et al. (1994) discovered 4U 0412+61, a new X-ray source with a 8.7s period. In all of the three cases, optical and infrared observations rejected the presence of a massive companion and also there was no evidence of orbital delays in pulse arrival times. Even if there exists a companion, its mass must have been extremely low. Due to these discrepancies from common pulsars, van Paradijs et al. (1995) described them as new class of objects and named them as "Anomalous X-ray Pulsars". AXPs are also observed to show SGR-like bursts but with certain differences. They have spectrally softer bursts than SGR-like bursts and a significant feature around 13 keV. The AXP bursts are correlated with pulse intensity, and total energy in tails of emission after burst is around or higher than the initial burst energy.

Since their calculated spin down luminosities are much less than observed luminosities, both SGRs and AXPs could not be rotation-powered pulsars. Also, the insufficient evidence of a massive companion implies that they

cannot be accretion–powered pulsars either. Ab initio models were inadequate explaining the tremendous bursts and repeating bursts at the same time. It has taken many years to entirely show that Soft Gamma Repeaters and Anomalous X-ray pulsars belong to the same group called magnetars (Gavril et al. 2004). Their spin periods are in a narrow range of 2-12s, and their spin down rates are high which implies that magnetic field at the surface of magnetars are several orders higher than that of ordinary radio pulsars. The high B-fields deduced from spin down rates are also confirmed independently by X-ray spectral model fits of the data (Perna et al. 2001). The timing age inferred from the spin down rates indicate that these objects are young neutron stars (1kyr–10kyr). Even though the timing age estimates may not be accurate due to timing noise of these objects, association of several magnetars with supernova remnants also confirm their age (Fahlman and Gregory 1981a). Magnetars also emit bright and sometimes variable X-ray photons with the luminosity of $10^{33} - 10^{36}$ ergs/s. They show prompt bursts with super–eddington luminosities (Kouveliotou 2003), reaching up to 10^{45} ergs/s within a several hundreds of milliseconds (Golenetskii et al. 1984). The pulse profiles of magnetars also show variability over time. Spectra of AXPs can often be modeled by black body plus a power law while SGR spectra are modeled with a single component which is either blackbody or power law model. In both cases, diminishing factor of interstellar absorption is also taken into account. Phase-coherent timing solutions of magnetars indicate that magnetar spin is not very stable. Some of the magnetars have been observed to possess glitches that are similar to those of radio pulsars but recovery time scales of those glitches are diverse. In this thesis, among all the magnetars, three most recently discovered SGRs will be studied for their X-ray their spectral features, period fluctuations and the timing noise associated with it.

CHAPTER 2

MODELS

2.1 Magnetar Model

Magnetar model first arose while trying to address the question “why do radio pulsars’ magnetic fields cluster around 10^{12} G?”. It was known that, pulsars emit radio beams through their magnetic poles as they also expel charged particles which bear off energy and angular momentum resulting in spin down for pulsars. What would happen if the magnetic field of a pulsar exceeds 10^{13} G? Because there is a critical value for magnetic field at

$$B_c = \frac{m_e^2 c^3}{e \hbar} = 4.4 \times 10^{13} \text{ G}. \quad (2.1)$$

If the magnetic field is stronger than this limit stated in Equation 2.1 which is known as quantum critical electrodynamic field strength, even the lowest energy state electrons revolve around the magnetic field lines at almost speed of light. This question is addressed by [Duncan and Thompson \(1992\)](#). They suggested that convective dynamo mechanism acting inside newly formed neutron star is the generator mechanism for high B-fields of magnetars.

They suggested that as it hosts free charged particles with neutrons, ultra-dense neutron star fluid may carry currents because the fluid itself is an electrical conductor. Since the fluid conducts electricity, magnetic field lines would sense any movement of the fluid. Therefore, the convective motions drift magnetic field lines which are trapped inside the fluid at the

very beginning of its creation. For a newly born fast rotating neutron star, dynamo action may generate magnetic fields up to 10^{16} G within the first 10 seconds of neutron star's life. After that period, convection and dynamo action will terminate, and the field is trapped inside the nucleon fluid. Dynamo mechanism enhances the initial magnetic field resulting in extreme B-fields (Thompson and Duncan 1996). Internal magnetic field is strained and it can be 10 times stronger than the external field. They further claimed that the ordinary radio pulsars possibly are not born with sufficient rotation speed to "trigger" large scale dynamos so that their magnetic field is rather low.

Soft Gamma Repeaters and Anomalous X-ray Pulsars are considered as observational reflections of the magnetar model (Woods and Thompson 2006) because the magnetar model is successful in explaining both persistent and burst emission mechanisms of SGRs and AXPs. According to their explanation, the persistent emission of magnetars are originated from the internal heating of magnetic field decay and twisting of the magnetosphere by the internal magnetic field. The internal heating increases the surface temperature to a value which is higher than the ordinary cooling neutron star with a comparable age. However, this effect can partially explain the persistency of emission of the magnetar. The internal magnetic field is twisted as it moves outwards and this movement also twists the magnetosphere giving a rise to persistent emission of the magnetar. The luminosities obtained from this mechanism are consistent with the observations and they may account for the luminosities higher than the spin down luminosities. The relaxations of the internal magnetic field can strain magnetar's crust, resulting in ruptures in the crust which is observationally associated with the short burst lasting for fractions of a second (Kouveliotou et al. 1998). Thompson and Duncan (1995) states that a SGR burst may originate from immense shifts of the magnetic field by magnetar's core. These large scale shifts will release vast amount of energy while readjusting itself to a lower energy state.

2.2 Fallback Disk Model

Another hypothesis that is put forward for explaining SGR and AXP emission mechanisms is fall back disk model. This model raises with an idea that a fossil disk should form around the neutron star just after the supernova explosion which forms the neutron star because all of the mass cannot be ejected during the supernova explosion and some of the initial mass will be "falling back" on to the neutron star (Chatterjee et al. 2000). The formed fossil disk will store the angular momentum and act like a "gyrostat" (Alpar 2001). The disk will be accreted back on to the neutron star, however; the accretion trajectory will not be continuous because the disk will truncate at Alfvén radius;

$$r_A \approx \mu^{4/7} \dot{M}^{-2/7} (GM)^{-1/7} \quad (2.2)$$

because magnetic pressure will become dominant over accretion pressure. Then the disk torque will cause spin down for the neutron star which can be deduced via (Alpar 2001):

$$I|\dot{\Omega}| \approx \mu^2 r_A^{-3} \approx \mu^{2/7} \dot{M}^{6/7} (GM)^{3/7} \quad (2.3)$$

According to that model evolutionary path of the magnetar is drawn by its dipole field. With rather low dipole fields (10^{12} - 10^{13} G) and the observed accretion rates that inferred from X-ray luminosities, it can explain period clustering of AXPs (Chatterjee et al. 2000). Even though, this model lacks in explaining burst phenomena of the AXPs and SGRs, once the burst initiated, impacts of the burst on the disk can explain post-burst luminosity enhancements in both IR and X-rays which are observed in some of the magnetars (Ertan et al. 2006). Fall back disk model implies 10^{12} - 10^{13} G surface dipole fields, while magnetar model requires a dipole field strength above the quantum critical value, the surface fields of magnetars are still unclear.

CHAPTER 3

INSTRUMENTS

3.1 RXTE

All the related information in this section is retrieved from, National Aeronautics and Space Administration (NASA), XTE Technical Appendix, Appendix F. The Rossi X-ray Timing Explorer (RXTE) is a satellite to observe timing properties of X-ray sources. It was launched by NASA's Goddard Space Flight Center 1995 December 30 and set into low Earth orbit (inclination 23 degrees). It is designed to observe fast X-ray variability of relatively bright sources. It can also observe spectral characteristics of X-ray sources with its moderate spectral resolution. Although RXTE can observe almost any point in the sky, there are some viewing restrictions. It cannot point below 30 degrees from the Sun. And it cannot perform observation during the South Atlantic Anomaly passage due to high energy particle flux. RXTE has three instruments attached (Figure 3.1); All sky monitor (ASM), Proportional Counter Array (PCA), and High Energy Timing Experiment (HEXTE).

3.1.1 PCA

The proportional counter array is built as a combination of five identical proportional counter units (PCUs). Each PCU is a xenon-methane gas proportional counter detector that are sensitive to photons in 2-60 keV range. Photons are detected via photoelectric effect when it interacts with

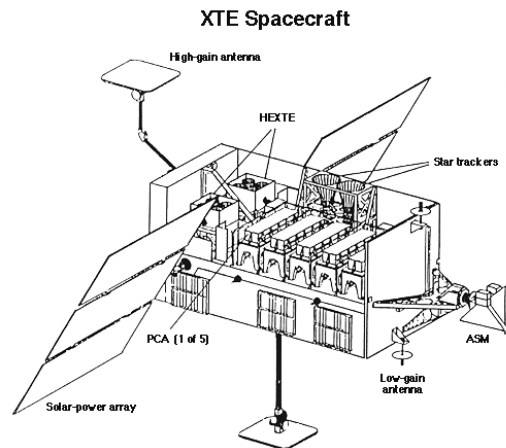


Figure 3.1. Schematics for RXTE instruments. Picture credit: RXTE/ASM home page.

the gas. The incident photon will detach an electron from the gas creating electron-ion pair. When there is a potential difference applied between anode and cathode, the primary detached electron move towards the anode, and ion will move towards cathode. Meanwhile electron will be accelerated by the applied potential difference, then it will interact with the gas again creating more pairs. However, ion will not gain enough kinetic energy due to its mass, thus it will be unable to create new pairs. The outgoing electrons will again follow the same process creating more and more electrons. This effect is known as Townsend avalanche. Ultimately, electrons will reach to the anode producing a signal. Total number of electrons reaching to the anode is linearly proportional to the energy of the photon that starts the Townsend avalanche. Methane gas used to avoid incorrect event recordings because sometimes xenon gas can be excited and emit a photon. And methane will absorb that photon without being ionized. Each PCU consists of five layers and below that layers there exists a Americium calibration source. Among those layers, top layer is the most sensitive, thus it will yield highest signal to noise ratio data. Because most of the X-ray events take place in the top layer. All the data are processed by on board micro-processor called the Experimental Data System (EDS) before telemetered to the ground.

PCA is capable of capturing photons over 2-60 keV energy range. It has

a large collecting area of 1400cm^2 each, totaling 7000cm^2 for 5 PCUs. Its main advantage is 1 microseconds time resolution. It possesses 256 energy channels and a moderate energy resolution ($<18\%$ at 6 keV). Field of view is 1 degree Full Width at Half Maximum (FWHM).

3.1.2 Data modes for pca

PCA data is registered in seven different Event Analyzer (EA) modes; burst catcher, single bit code, fast Fourier transform, pulsar-fold, delta binned, event encoded, and binned data modes. There are also several configurations related to each mode. In this thesis, relevant EA modes used are event encoded mode and binned data mode.

Event encoded mode outputs a list of arrival times for each event with maximum time resolution of RXTE (1microsec). It allows selection for which PCU or layer to use. There are three configurations for this mode, Good Xenon, GoodXenon with Propane, and Transparent. GoodXenon configuration provides all events except from events that are marked as background. It also have all 256 energy channel of PCU, allowing user to filter necessary energy ranges. Good Xenon with Propane is almost same with previous one except the fact that it also records propane layer events. Transparent configuration returns all the events occurred during the observation, therefore events related with source or background are indistinguishable. Accordingly, obtained data from this configuration is not appropriate for analysis.

Binned data mode returns times series with certain bin time depending on configuration. In this data mode, only the data unmarked as background are recorded. Standard-1 and Standard-2 are the configurations for this data mode. Standard-1 is binned with 0.125 seconds and possesses no energy resolution because data is integrated over all energy channels. Standard-2 is however, has 16 seconds bin time. It sets 256 energy channels to 129 energy channels and user is free to filter among them.

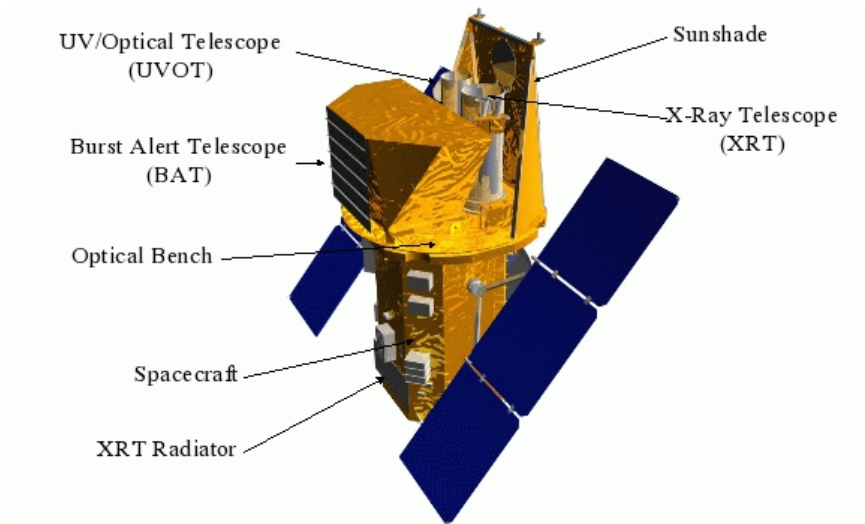


Figure 3.2. Schematics for SWIFT instruments. Picture credit: SWIFT home page.

3.2 SWIFT

The information of technical overview of SWIFT satellite is obtained from NASA, Swift Technical Handbook, Appendix F. The Swift is a multi-wavelength mission covering optical, ultraviolet, X-ray and gamma-ray bands of electromagnetic spectrum (see Figure 3.2). The satellite is initiated as one of medium explorer program of NASA and was launched on 2004 November 20. It was set move in low-Earth orbit. Main goal of the project is to accelerate GRB science. It carries three instruments on board; Burst Alert Telescope (BAT), X-ray Telescope (XRT), Ultraviolet-Optical Telescope (UVOT). All the instruments attached works in tandem with each other, It can locate position of the source with 3 arcminutes accuracy within 20 seconds after a burst detection and can point XRT and UVOT to the source in 90 seconds. And all the data acquired is available for public use as soon as its reprocessed.

3.2.1 XRT

XRT is built upon already existing JET-X hardware which is functioning as optical bench used for aligning X-ray mirrors and focal plane detectors. It

has a 100cm^2 effective area and 23.6×23.6 arcminutes field of view. XRT can collect photon within 0.2-10 keV energy band. Photons are detected via CCD with 600×602 pixels of image area. Energy resolution at FWHM is 190 eV at 10 keV, decreasing to 50 eV at 0.1 keV. Optimal temperature that CCD operates is around -100 degree Celsius in order to obtain low dark current and reduce CCD's sensitivity to irradiation by protons. XRT observations held in three different modes; Imaging, Photon Counting (PC), and Windowed Timing. In imaging mode, CCD image is integrated recording total energy per pixel. Therefore, Imaging mode data is unable for spectral analysis purposes. But in this mode, bright sources can be localized with sub-second uncertainty in detector coordinates corresponding to 5 arcseconds uncertainty radius in sky coordinates. Photon Counting mode functions by sub-array windows allowing maximum spectral and spatial information. Windowed Timing mode events are compressed into 1 dimensional image by binning 10 rows to a single row. Time resolution obtained by WT mode is $1700\mu\text{s}$.

3.3 XMM-Newton

In this section, the technical details of XMM-Newton satellite is retrieved from http://xmm.esac.esa.int/external/xmm_user_support/documentation/technical/Spacecraft/index.shtml, XMM-Newton: A Technical Design, maintained by European Space Agency (ESA). An Ariane-504 launched X-ray Multi Mirror Mission (XMM-Newton) on December 10th 1999. XMM-Newton carries three X-ray telescopes and each of them consists of 58 Walter I grazing incidence mirrors. The optical system was designed in order to obtain the highest possible effective area over a wide range of energies that is around 7 keV. Focal length of the telescopes is 7.5 m and the longest mirror has 70 cm diameter. Also, each telescope has 1550 cm^2 geometric area at 1.5 keV. Investigation of spectra of cosmic sources with X-ray fluxes as low as $10^{-15}\text{ erg cm}^{-2}\text{ s}^{-1}$ (Jansen et al. 2001), acquiring sensitive medium-resolution spectroscopy with resolving powers between 100

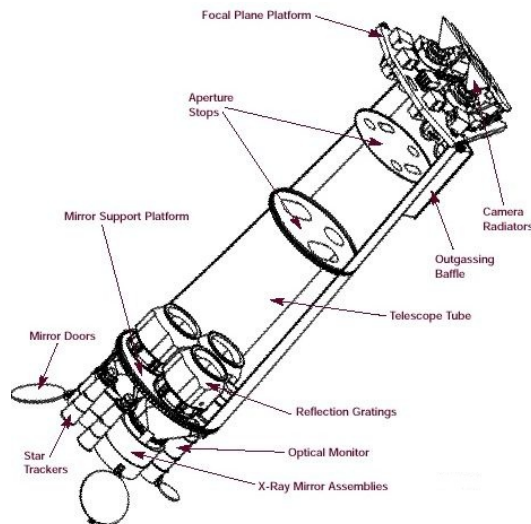


Figure 3.3. Schematics for XMM instruments. Picture credit: ESA/XMM home page.

and 700 over the wavelength band 350-2500 eV, broadband imaging spectroscopy from 100 eV to 15 keV, and multi-wavelength studies between 1600-6000 Å with a designated optical monitor are the main objectives of the mission (Wenzel 2003). The 4 tone, 10 mm long XMM-Newton satellite includes three main instruments on board (Figure 3.3);

- European Photon Imaging Corneas (EPIC)
- Reflection Grating Spectrometers (RGS)
- The Optical Monitor (OM)

There are three CCDs operating that is on the focal plane of Walter-Type X-Ray telescopes for X-ray imaging, medium-resolution spectroscopy and photometry. Two of them are called EPIC-MOS (Metal Oxide Semiconductor) and the last one is EPIC-PN. EPIC-MOS includes 7 CCDs that have 40 μm pixel size. EPIC-PN consists of 12 CCDs that have 150 μm pixel size. The cameras have capability of measuring the arrival time, impact position on the detector and the energy of X-Ray photons. The RGS have an array of reflection gratings that diffracts the X-Rays to the array of dedicated CCDs. High resolving power that is from 150 to 800 is obtained by RGS over a range from 5 to 35 Å. Optical monitoring enables to observe

simultaneously in the X-Ray, UV and optical wavebands. The OM covers a wavelength range between $170\mu\text{m}$ and $650\mu\text{m}$ of the central 17 arcmin square region of the X-ray field of view.

3.3.1 Operating modes

EPIC cameras give some opportunities in order to acquire data. The CCDs of MOS cameras are used in full frame imaging mode; on the other hand, PN camera CCDs can be run for full frame, extended full frame, partial window mode and timing mode. In the full frame and extended full frame mode all pixels of all CCDs are read out, therefore, the full field of view is covered. The partial window mode can be operated as small window mode and large windows mode. The central CCD of the MOS cameras can be operated in a different mode by reading out part of the CCD and an area of 100×100 pixels is read in small window mode while an area of 300×500 pixels is read in large window mode. For PN cameras, half of the area of all 12 CCDs is used in large window mode, whereas CCD0 in quadrant is read out to collect data. In timing mode, the data is collapsed into one dimensional raw in order to increase high time resolution. Moreover, there is another mode for only PN camera which is called Burst mode. In this mode time resolution is very high but it has a low duty cycle of %3.

3.3.2 EPIC

EPIC MOS and PN cameras are built for observing photons with an energy range from 0.15 keV to 15.0 keV. Field of view of the telescope is 30 arcmins and it has 20-50 spectral resolution and 6 arcsec at FWHM angular resolution. The data obtained within the imaging mode should be reprocessed due to photons which are detected at the time of read-out, these photons may confuse the frame and spectral features may be broadened. Additionally, the data should be checked for whether pile-up exists or not, especially in the case of analyzing extended objects. The pile-up may lead data loss

as it causes loss of the incoming flux. However, point-like-sources can be analyzed smoothly even if there exists pile-up.

3.4 CHANDRA

The details of technical overview for Chandra X-ray Observatory is adapted from The Chandra Proposers' Observatory Guide written by Chandra X-ray Center (CXC). Chandra X-ray Observatory, which was launched on July 23 1999, can perform observations up to 55 hours without a break and completes its elliptical orbit in 63.5 hours. Optics of the telescope composed of iridium coated Walter Type-I grazing incidence X-ray mirrors such as XMM-Newton. Effective area of the telescope is 400 cm^2 at 5 keV and the focal length is 10.066 m. Satellite orbits above the radiation belts more than 75 percent of its complete orbital time. See Figure 3.4 for the schematic of the satellite and its instruments. Science instruments are

1. High Resolution Camera (HRC)
2. Advanced CCD Imaging Spectrometer(ACIS)
3. High Resolution Spectrometers
 - Low Energy Transmission Grating (LETG)
 - High Energy Transmission Grating (HETG)

ACIS and HRC are the focal plane instruments which are capable of capturing the image of incoming X-rays and provide information about their position, number, energy and time of arrival. HRC has two micro channel plate detectors which are formed the array of several electron multipliers. These multipliers work with basic physical process like photoelectric effect.

One of the detectors, HRC-S, is for grating spectra which has a spectral range of $0\text{-}160 \text{ \AA}$, works in the energy range of $0.08\text{ - }6 \text{ keV}$ and its FOV is $6 \text{ arcmins} \times 99 \text{ arcmins}$. The other one is for wide-field imaging (HRC-I) which works in the energy range of $0.1\text{-}10 \text{ keV}$ with a spectral range of $0\text{-}60 \text{ \AA}$ and its FOV is $30 \text{ arcmins} \times 30 \text{ arcmins}$.

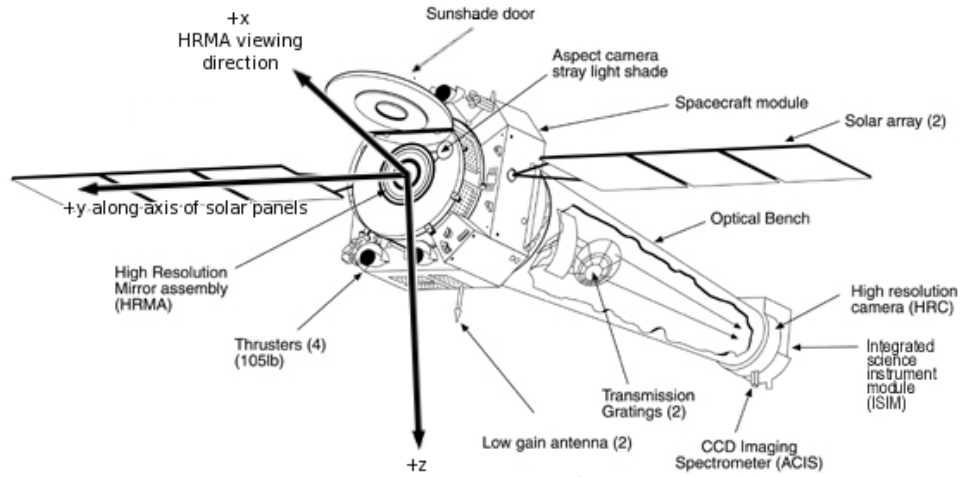


Figure 3.4. Schematics for Chandra instruments. Picture credit: Chandra/CXC home page.

HETG provides for high resolution spectroscopy between 0.4 - 8.0 keV with resolving power up to 1000. It consists of two gratings called Medium Energy Grating (MEG) and High Energy Grating (HEG). MEG has an energy range of 0.4 – 5.0 keV with a wavelength range of 31 – 2.5 Å. Its energy resolution is 0.023 Å at FWHM while for HEG, it's 0.012 Å. HEG has an energy range of 0.8 – 10.0 keV with a wavelength range of 14 – 1.2 Å. HETG has an effective area of 7 cm² at 0.5 keV.

Even though LETG and HETG share a similar design, LETG is specifically modified for the energies up to 1 keV and also it mostly operates with HRC-S and ACIS-S. The LETGS provides studies of spectral line profiles by using high-resolution spectroscopy $\frac{\lambda}{\Delta\lambda} > 1000$ over the range of 0.07 – 0.15 keV, energy resolution of 0.05 Å at FWHM and moderate resolving power at shorter wavelengths.

ACIS is composed of two arrays, ACIS-S and ACIS-I, with one array designed to optimize imaging, spectrometry and high resolution spectroscopy by working together with HETG and LETG, and the other array for spectroscopy utilizing, imaging and spectrometry. ACIS-S has 6 CCDs (1024 × 1024 pixels) and ACIS-I has 4 CCDs, all connected to their individual CCD controllers. ACIS has two operating modes:

- Timed Exposure Mode (TE)
- Continuous Clocking Mode (CC)

3.4.1 Timed Exposure Mode (TE)

This mode collects data within a certain time frame between 0.2 to 10 seconds and transfers the data at the end of each time frame. When all CCDs are operational, frame time for each is 3.2 seconds, however, if frame time is shorter than the given time, dead times will occur which results in no data taken. And a frame time longer than 3.2 seconds increases the probability of a possible pile-up.

The nominal time for each CCD can be changed by selecting a region of an individual CCD, which recalled subarrays, rather than changing the full frame. This specific nominal time depends on the number of rows in the subarray, total number of activated CCDs and the number of rows between subarray and frame-store regions. Differences between the nominal time frame and the selected time frame on the subarray, results in same effects as the full frame.

3.4.2 Continuous Clocking Mode (CC)

The Continuous Clocking (CC) mode can acquire data with 3 msec read out time giving up the spatial resolution. The CC mode generates 1 pixel \times 1024 pixels images at each read out. The time recordings taken in this mode are not arrival times of the photons but they are read out recordings for level 1 data. Time between them may differ 2.9–5.8 s due to location of the source on the CCD. Therefore these data recordings should be reprocessed to correct arrival times or level 2 files should be used.

CHAPTER 4

SOURCES AND OBSERVATIONS

4.1 Selected Sources

4.1.1 SGR J1833–0832

On 2010 March 19, a typical short SGR burst of hard X-rays triggered Burst Alert Telescope (BAT) of an on board satellite called the SWIFT from a source located near the galactic plane ([Barthelmy et al. 2010](#)). The burst spectrum of SGR J1833–0832 resembles of those known magnetars and it can also be modeled by either a blackbody emission with $kT = 10$ keV or a power law model with an exponential cut off. The source location was determined with 1.6' accuracy, and it was not coinciding with any known SGR. Later on, the source location was found more precisely by CHANDRA ACIS-I observations and its location R.A. = 18h 33m 44.37s, DEC. = -08d 31' 07.5" (J2000) with a 0.4 arcseconds of accuracy ([Gogus 2010](#)). Subsequent observations of RXTE showed 7.56s coherent X-ray pulsations which confirms the SGR nature of this new source ([Palmer and Gelbord 2010](#)), ([Gogus et al. 2010](#)). The Swift UVOT observations ruled out the presence of a source in UV and optical band within the refined XRT position ([Marshall and Gelbord 2010](#)). The search for IR counterpart with VLT/HAWKI revealed no existing source in 22.4 magnitude upper-limit ([Göğüş et al. 2010](#)). [Burgay et al. \(2010\)](#) sought for radio emission using the Australia Telescope Compact Array and the Parkes Radio Telescope, no significant radio emission was detected at 1.5 GHz and 1.4 GHz frequencies with an

upperlimit flux densities of 0.9 mJy and 0.09 mJy respectively. [Gögüş et al. \(2010\)](#) published the spin down rate history spanning for 50 days and [Esposito et al. \(2011\)](#) expanded it to 225 days since the outburst.

4.1.2 SWIFT J1822.3–1606

The SWIFT J1822.3–1606 was discovered through a BAT trigger of the SWIFT satellite on 2011 July 14 ([Cummings et al. 2011](#)). The trigger was originated by a burst of hard X-ray emission from a source that is not known yet. Immediately after the burst, location of the source is found to be at RA = 18h 22m 18.00s and DEC = –16d 04' 26.8" with an uncertainty radius of 1.8 arcseconds using the SWIFT– XRT ([Pagani et al. 2011](#)). The spin period of the pulsations is determined to be 8.4377s ([Gogus et al. 2011b](#)). Initially, the SWIFT J1822.3–1606 was thought to be an Be/X-ray binary due to its similarities with the Be/X-ray binary J1626–5156 ([Gogus et al. 2011c](#)). However, the lack of evidence of optical counterpart confront the idea of source being a Be/X-ray binary ([Rea et al. 2011](#)). Magnetar nature of the SWIFT J1822.3-1606 is soon confirmed with its timing properties ([Livingstone et al. 2011](#)). Distance of SWIFT J1822.3-1606 is estimated 1.6 ± 0.3 kpc, making it one of the closest magnetars ([Scholz et al. 2012](#)). [Rea et al. \(2012\)](#) claimed that source was already detected in quiescent state in the archival ROSAT image before the burst. And they also searched for multi-wavelength emission from the source. They reported that radio observations using Green Bank Telescope did not reveal any radio counterpart for the source. They also initiated optical and infrared observations with Gran Telescopio Canarias on 2011 July 21 and couldn't find any source associated with given coordinates. Its X-ray timing and spectral properties are already presented for 84 days ([Livingstone et al. 2011](#)) and 260 days ([Rea et al. 2012](#); [Scholz et al. 2012](#)). [Rea et al. \(2012\)](#) found that timing solutions of the source have relatively high root mean square value, implying noisy structure of its timing parameters.

4.1.3 SWIFT J1834.9–0846

Discovery of Swift J1834.9–0846 came on 2011 August 7 with a SGR-like burst triggered BAT (D'Elia et al. 2011). The source repeated the burst for the second time almost 3 hours later, this burst also triggered the Gamma Ray Burst Monitor (GBM) of FERMI satellite (Guiriec et al. 2011). Following the burst, RXTE observations on 9 – 10 August revealed a coherent signal with 2.4822 s period, making it one of the fastest spinning magnetars (Gogus and Kouveliotou 2011). Moskvitin et al. (2011) detected an object in the optical band with 23.44 ± 0.34 magnitude, however; its position did not match with precise X–ray source position determined from the subsequent CHANDRA observations, RA = 18h 34m 52.12s, Dec = -08d 45' 55.97" with 0.60 arcseconds uncertainty (Gogus et al. 2011a). Observations with Palomar Hale telescope ruled out presence of an IR counterpart down to 19.5 magnitude (Kargaltsev, O. and Kouveliotou, C. and Pavlov, G. G. and Göğüş, E. and Lin, L. and Wachter, S. and Griffith, R. L. and Kaneko, Y. and Younes, G. 2012) . As it located in supernova remnant SNR W41, association with that SNR is still an open question (Kargaltsev, O. and Kouveliotou, C. and Pavlov, G. G. and Göğüş, E. and Lin, L. and Wachter, S. and Griffith, R. L. and Kaneko, Y. and Younes, G. 2012). If it is indeed born in that SNR, distance of the magnetar is estimated to be around 4 kpc. Calculated pulsed fraction of the source is unusually high among magnetars, 85 ± 10 (Kargaltsev et al. 2011). CXO image of the source is not consistent with point spread function, thus implying an extended emission, probably from dust scattering halo. Younes et al. (2012) argued that extended emission around that magnetar is attributed to two different emission mechanism, dust scattering halo and possible magnetar wind nebulae (MWN). Timing solution of the source is reported in literature spanning 30 days (Kargaltsev, O. and Kouveliotou, C. and Pavlov, G. G. and Göğüş, E. and Lin, L. and Wachter, S. and Griffith, R. L. and Kaneko, Y. and Younes, G. 2012).

4.2 Observations

In Table 4.1 journal of observations for all selected sources from all satellites are given.

Table 4.1. Journal of RXTE observations. SAT is the satellite observation carried out; N is number of observations; T is total exposure time in ksec.

SAT	Object	N	T
RXTE	SGR J1833–0832	81	462.031
RXTE	SWIFT J1822.3–1606	34	178.862
RXTE	Swift J1834.9-0846	17	106.400
SWIFT	SGR J1833–0832	27	259.459
SWIFT	SWIFT J1822.3–1606	38	100.797
SWIFT	Swift J1834.9-0846	3	5.945
XMM-Newton	SGR J1833–0832	3	65.023
XMM-Newton	Swift J1834.9-0846	1	28.917
Chandra	SGR J1833-0832	1	33.550
Chandra	SWIFT J1834.9-0846	1	14.350

4.2.1 RXTE Observations

SGR J1833–0832 is observed by RXTE between 2010 March 19 and 2010 December 3 during which the source is detectable. We used 81 observations with a total exposure of 462 ks. RXTE observations for SWIFT J1822.3–1606 were held between July 14, 2011 and November 28, 2011. During that time interval, the source has been monitored 34 times yielding a total exposure of 179 ks. RXTE pointed for coordinates of Swift J1834.9–0846 for 17 times. These observations have a total 106 ks exposure between 2011 August 9 and 2011 December 4 (Table 4.1).

All the data were obtained using the PCA detector in GoodXenon mode which has a time resolution of 1 microseconds. For timing analysis, we created the lightcurve in 2-10 keV range with 0.05 seconds of binning. Then, we subtracted background from the lightcurve using the PCA background model. All the photon arrival times in the lightcurve are corrected

to solar system barycenter using `fxbary` command on `ftools`. Finally, data is corrected for all the PCUs. We tried to obtain spectrum of the source using standard 2 mode data, however; since RXTE is not a focusing instrument and the field is crowded by other sources, obtained spectrum was not suitable for spectral analysis.

4.2.2 SWIFT Observations

We analyzed 27 pointing observations of SWIFT satellite of SGR J1833–0832. Data spans for more than 5 months between 2010 March 19 and 2010 August 27. Among those 27 observations, 26 of them were done with photon counting mode and only 1 observation was done with XRT windowed timing mode. SWIFT J1822.3–1606 was observed continuously for almost 6 months (between 2011 July 16 and 2012 February 28) during which SWIFT has taken 38 pointing observations. All of them was on windowed timing mode except 3 which are held in photon counting mode. Total exposure for the WT mode observations were about 83 ks. Observations for SWIFT J1834.9–0846 were held between 2011 August 07 and 2011 September 24, during which SWIFT has taken 20 pointings, yielding 74 ks exposure in total (Table 4.1). Three of those pointings were on PC mode and rest were on WT mode. Since the windowed timing mode does not have high energy resolution, we have omitted that observations from our spectral analysis of our sources. We have reprocessed the data using `XRTPIPELINE` and filtered with `FTOOLS` in the `HEASOFT` package. Centering on the source, circular region with 20 pixels radius was used to extract the source events and the annular region between 40 and 50 pixels radius was used to extract background events. For timing measurements we only used WT mode data to obtain lightcurves. As the pulse profiles depends on energy bands for our sources, energy range for photon selection in events were at 2-10 keV to make it consistent with pulse profiles obtained by other instruments.

4.2.3 XMM-Newton Observations

We used the 3 public XMM-NEWTON observations of SGR J1833–0832, 65ks in total, from HEASARC data archive. Two of the observations were made in Full Frame mode of EPIC Camera and one observation was performed in Large Window Mode of MOS. Even though SWIFT J1822.3–1606 observed by XMM-Newton, none of these data were public. Therefore we were not able to analyze any of them. Satellite also pointed Swift J1834.9–0846 on 2011 September 17 for 24ks (Table 4.1). Both EPIC-MOS and EPIC-PN detectors were operating simultaneously during the observation with Small Window mode and Full Frame mode respectively. Data were processed with standard filtering and screening criteria using XMM–NEWTON Science Analysis Software (SAS). Circular region of 40 arcseconds radius is used to extract the source events from the data and region for the background events are chosen from source-free region with 80 arcseconds radius. Spectral analysis are carried out with the ancillary response files created by ARFGEN task and the spectral redistribution matrices created by RMFGEN task of XMM–NEWTON Science Analysis Software.

4.2.4 CHANDRA Observations

SGR J1833–0832 was on focus of Chandra satellite for 33 ks on 2010 March 23. Observation pointing was done using ACIS-I camera of the on board satellite. There are 6 observations for SWIFT J1822.3–1606 source and 4 observations for Swift J1834.9–0846 in the HEASARC archive, however; those archived observations were unpublic to use except from 1 observation of Swift J1834.9–0846 (table 4.1). We processed the data using Chandra Interactive Analysis of Observations (CIAO) software. We selected photons centering on our source within 20 pixels circular region as our source events. Background events are extracted from 40 pixels radius from source–free region. Then we created spectrum and response files by running specextract script within CIAO software.

CHAPTER 5

DATA ANALYSIS AND RESULTS

5.1 Phase coherent timing

Magnetars are stable rotators like pulsars however, they spin down more rapidly. Their rotation periods as function of time can be estimated very accurately over the years. As its discussed in the previous chapters, magnetars are thought to be spinning down due to their magnetic field, thus spin down measurements favor to approximate its dipolar field.

For timing measurements, satellite observations are taken continuously during many pulse cycles. The starting time of observations and the moment each photon arrives are recorded with high precision. The output time series is registered as data for observations. The time recordings are required to be transformed to Solar System barycenter so that arrival time of photons can be assumed to be observed in inertial reference frame. However, for this transformation, precise determination of sky coordinates is necessary. Then, the recorded data is folded over a period of pulsations resulting in an average pulse profile for a given source. Avarage pulse profiles are then represented as harmonics in order to obtain highest possible precision for both phase and noise estimations in pulse waveforms (Deeter and Boynton 1982). A typical representation of the pulse frequency as a function of time can be expressed as follows:

$$\nu(t) = \nu_0 + \Delta\nu(t) \tag{5.1}$$

Assuming that pulse frequency $\nu(t)$ is not varying over the entire observa-

tion span, pulse phase can be written in the form of:

$$\phi(t) = \nu_0(t - t_0) + \Delta\phi(t) \quad (5.2)$$

where $\Delta\phi(t)$ is small, and not changing significantly. To obtain the spin down history of the source, first barycentered time series is folded over the spin frequency, output is called pulse profile. Folded over the pulsation period, typical harmonic representation for pulses can be denoted as truncated Fourier series:

$$g(\phi) = G_0 + \sum_{k=1}^m G_k \cos k(\phi - \phi_k) \quad (5.3)$$

After each observation is folded over the source period, the pulse profile for each observation is constructed. One must first have to determine the template pulse profile in order to use it as a reference for the rest of the independent sample pulses. The template or master pulse is determined from the longest observation that gives best reduced chi-squared. Then all the independent sample pulses are defined as:

$$f(\phi) = F_0 + \sum_{k=1}^m F_k \cos k(\phi - \phi_k + \Delta\phi_k) \quad (5.4)$$

Assuming there exists a white noise for the pulse shape, phase difference between template pulse and sample pulse can be determined from searching for the maximum value in the cross-correlation among them. Using the orthogonality of harmonics phase offsets between two pulses can be written in the form of:

$$\Delta\phi = \frac{\sum_{k=1}^m k G_k F_k \sin k \Delta\phi_k}{\sum_{k=1}^m k^2 G_k F_k \cos k \Delta\phi_k} \quad (5.5)$$

And to approximate pulse frequency derivatives, these phase offsets can be modeled as a Taylor series expansion:

$$\delta\phi = \phi_0 + \delta\nu(t - t_0) + \frac{1}{2}\ddot{\nu}(t - t_0)^2 + \frac{1}{6}\dddot{\nu}(t - t_0)^3 + \dots \quad (5.6)$$

The determined timing solution from above equation is used to align pulses with minimum possible residuals. And using the pulse profiles, one can

also determine pulsed fraction of the incoming emission. Pulsed fractions in this thesis are calculated using the equation below:

$$PulsedFraction = \frac{C_{max} - C_{min}}{C_{max} + C_{min}} \quad (5.7)$$

where C_{max} and C_{min} refers to maximum and minimum count rates of pulse profile bins. And corresponding uncertainties in pulsed fraction calculations are determined by mean error of phase bins. We used the following equation to account for uncertainties.

$$\Delta(PulsedFraction) = \frac{4 \Delta C C_{max}}{(C_{max} + C_{min})^2} \quad (5.8)$$

Once the timing parameters of the source is determined, magnetic field at the surface of the neutron star can be estimated via dipole braking formula:

$$B = 3.2 \times 10^{19} \sqrt{P\dot{P}} \text{ G}. \quad (5.9)$$

5.1.1 SGR J1833–0832

[Esposito et al. \(2011\)](#) published the spin down history for SGR J1833–0832 covering a time span of almost 225 days since the initial burst leading to its discovery. They found 7.5654091s coherent pulsations with a spin down rate of $4.39 \times 10^{-12} \text{ s s}^{-1}$. We also performed phase coherent timing analysis for this source to observe long term variations of its timing characteristics.

In order to obtain timing parameters of SGR J1833–0832, we used only RXTE-PCA observations which extend until 257 days since the discovery of the source. Lightcurve is created from those observations with prevalent filtering options within 3–20 keV energy band. Contribution of background emission is estimated via default background models prepared by RXTE-PCA team. Background estimations are modeled with PCABACKEST command and the resulting background model is subtracted from the lightcurve. Then, time column of the light curve is corrected to the Solar System barycenter and the count rates are scaled for all the PCUs. We

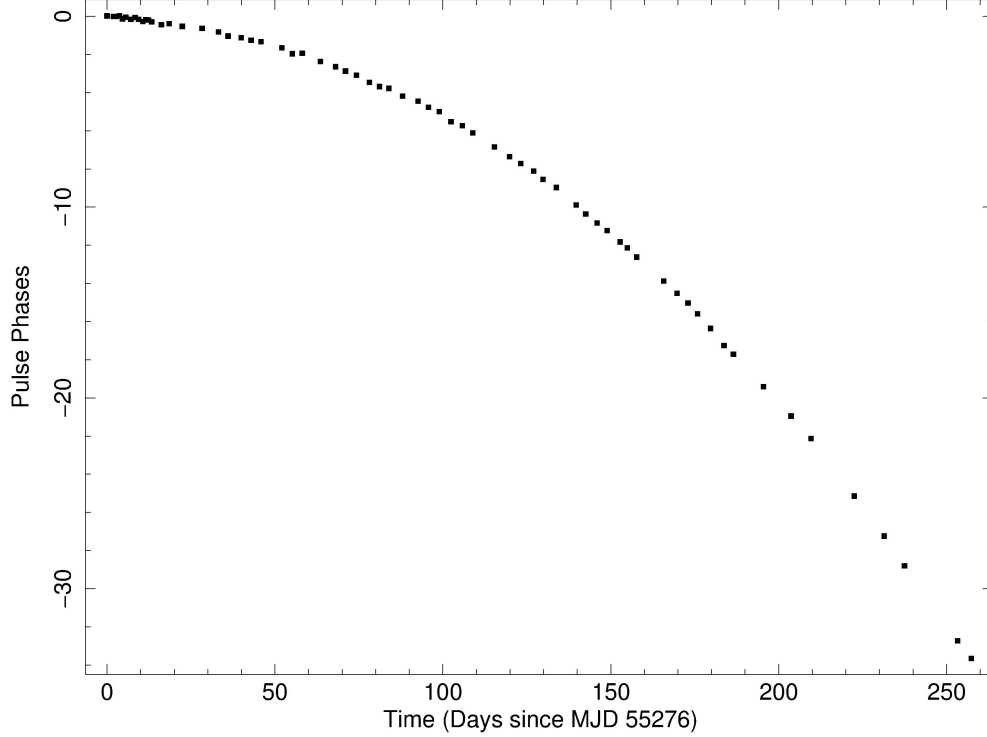


Figure 5.1. Pulse arrival times of SGR J1833–0832

constructed pulse profile for each observation unless they are subsequently observed within 24 hours. If more than one observation occurred in same day, those observations combined into one.

The normalized pulse profiles are then held subject to cross-correlation for pulse timing analysis. Our timing solutions yield a coherent signal at $\nu = 0.1321807598$ Hz with a frequency derivative of $\dot{\nu} = -1.35296544 \times 10^{-13}$ Hz/sec (Figure 5.1). Assuming that spin period of the source is slowing down due to dipole braking, those timing values correspond to a magnetic field of 2.45×10^{14} Gauss at the surface of the magnetar (Table 5.1). The obtained timing parameters are consistent with the values reported earlier

Table 5.1. Timing parameters of SGR J1833–0832

Parameter	Value
Epoch (MJD)	55276.64
Spin frequency (Hz)	0.1321807598(8)
Spin down rate (Hz/s)	$-1.352(9) \times 10^{-13}$
Inferred dipole field strength (Gauss)	2.45×10^{14}

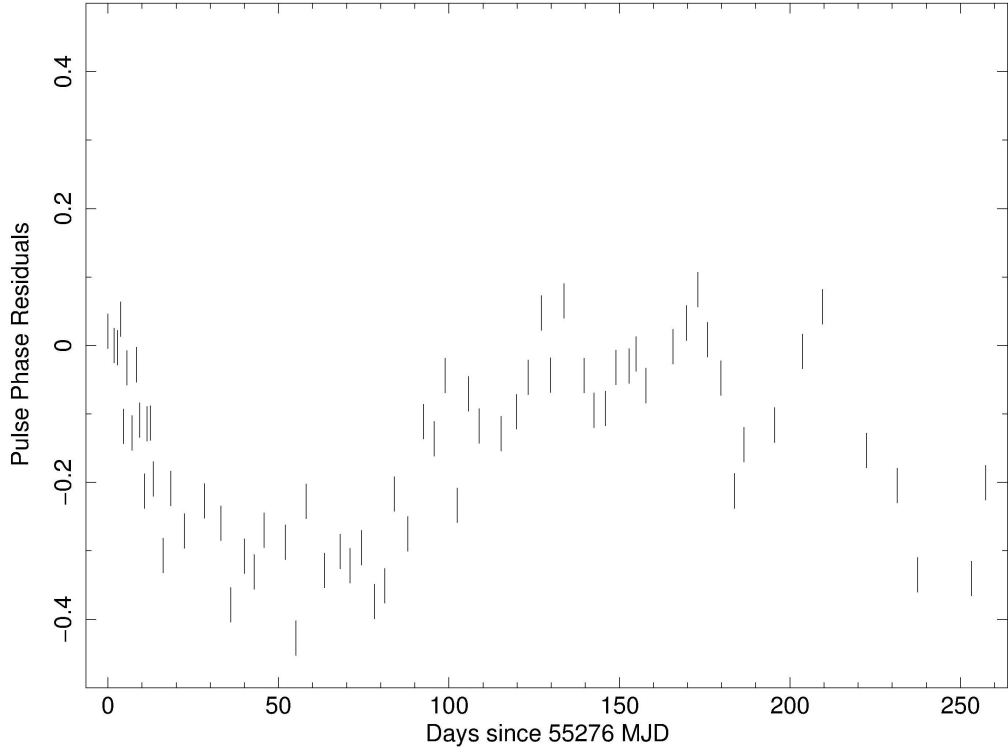


Figure 5.2. Timing residuals of SGR J1833–083

(Esposito et al. 2011; Kuiper and Hermsen 2011) which implies that SGR J1833-0832 is still steadily spinning down without a glitch until it reaches to the quiescent state. Figure 5.2 illustrates the residuals of the pulse arrival times after the removal of quadratic polynomial.

5.1.2 SWIFT J1822.3-1606

For SWIFT J1822.3-1606, both Swift-XRT and RXTE-PCA observations are used for obtaining maximum time span so that the timing parameters of the source can be estimated more accurately. RXTE lightcurve is generated with standard filtering criteria presented in HEASOFT package in FTOOLS. Background emission is modeled and subtracted from the original lightcurve to obtain net source lightcurve. Then the barycentric correction is applied to the time series presented in the lightcurve and its also corrected for all the PCUs by means of their on/off time. Swift–XRT lightcurve is created only from WT mode observations because PC mode observations have insufficient time resolution to carry out pulse timing analy-

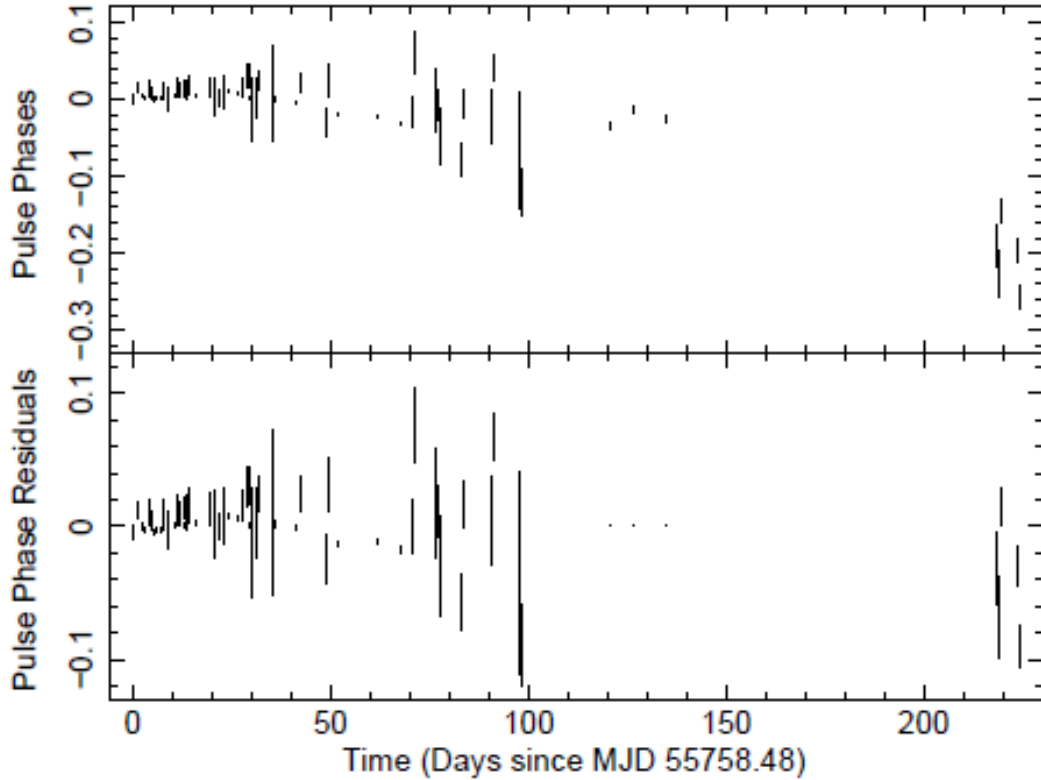


Figure 5.3. Pulse arrival times of Swift J1822.3-1606

sis. Those observations are reprocessed with XRTPIPELINE command and filtered regarding standard options. Time series in the event file are converted to Solar System Barycenter. We used 16 pixel strip to extract source events from the reprocessed events image. Then, we created background subtracted lightcurve with 0.05s binning.

Both lightcurves are constructed within same energy band 2-10 keV in order to avoid energy dependent pulse profile variability which would cause unintended errors while cross-correlating individual pulse profiles. All the pulse profiles are normalized and cross-correlated to acquire phase off-

Table 5.2. Timing parameters of Swift J1822.3–1606

Parameter	Value
Epoch (MJD)	55758.48
Spin period (s)	8.437720238(9)
Spin down rate (s/s)	$5.98(3) \times 10^{-14}$
Inferred dipole field strength (Gauss)	2.2×10^{13}

sets (Figure 5.1.2). Resulting offsets are then modeled by Taylor expansion that is mentioned in previous section. It yields a frequency of $\nu = 0.1185154250(9)$ Hz corresponding to a spin period of 8.43772023(5) s. And the magnetar SWIFT J1822.3-1606 is spinning down at the rate of $\dot{P} = 5.98(3) \times 10^{-14}$ s/s, which implies a dipolar field of 2.2×10^{13} G at the surface of the magnetar (Table 5.2). Inferred dipole field strength for this source is lower than quantum electrodynamical field strength, suggesting that true emission mechanism for magnetars may not directly associated with the inferred dipolar field but the torodial field inside the magnetar. We saw that residuals of this timing solution is rather noisy which could be attributed to either torque noise that is correlated with an accretion or existence of a second frequency derivative. For the latter case, we added second frequency derivative in order to minimize the residuals of timing solution. The former case will be interpreted in the section 2 of Chapter 5.

5.1.3 Swift J1834.9-0846

Pulse timing analysis of Swift J1834.9-0846 is carried out using RXTE-PCA observations which are between August 9 and December 4 2011. All the observations are held subject to standard procedure for filtering. We extracted a lightcurve selecting photons with energy range of 2-10 keV. The lightcurve count rates are corrected for all PCUs and the time series are converted to barycentric dynamical time using refined source coordinates obtained from CHANDRA observations.

Obtained lightcurve is folded over spin period $P = 2.48230033$ s of the magnetar using epoch as 55783 MJD. Resulting pulses are investigated for energy and time dependency. Profiles are not varying over energy ranges but changing with time. To illustrate its time dependency, we created 8 pulse profiles from different observations which are presented in the Figure 5.1.3.

Pulse timing analysis for the Swift J1834.9-0846 magnetar source revealed a spin down rate of $\dot{\nu} = -1.462(2) \times 10^{-12}$ Hz/sec corresponding to a mag-

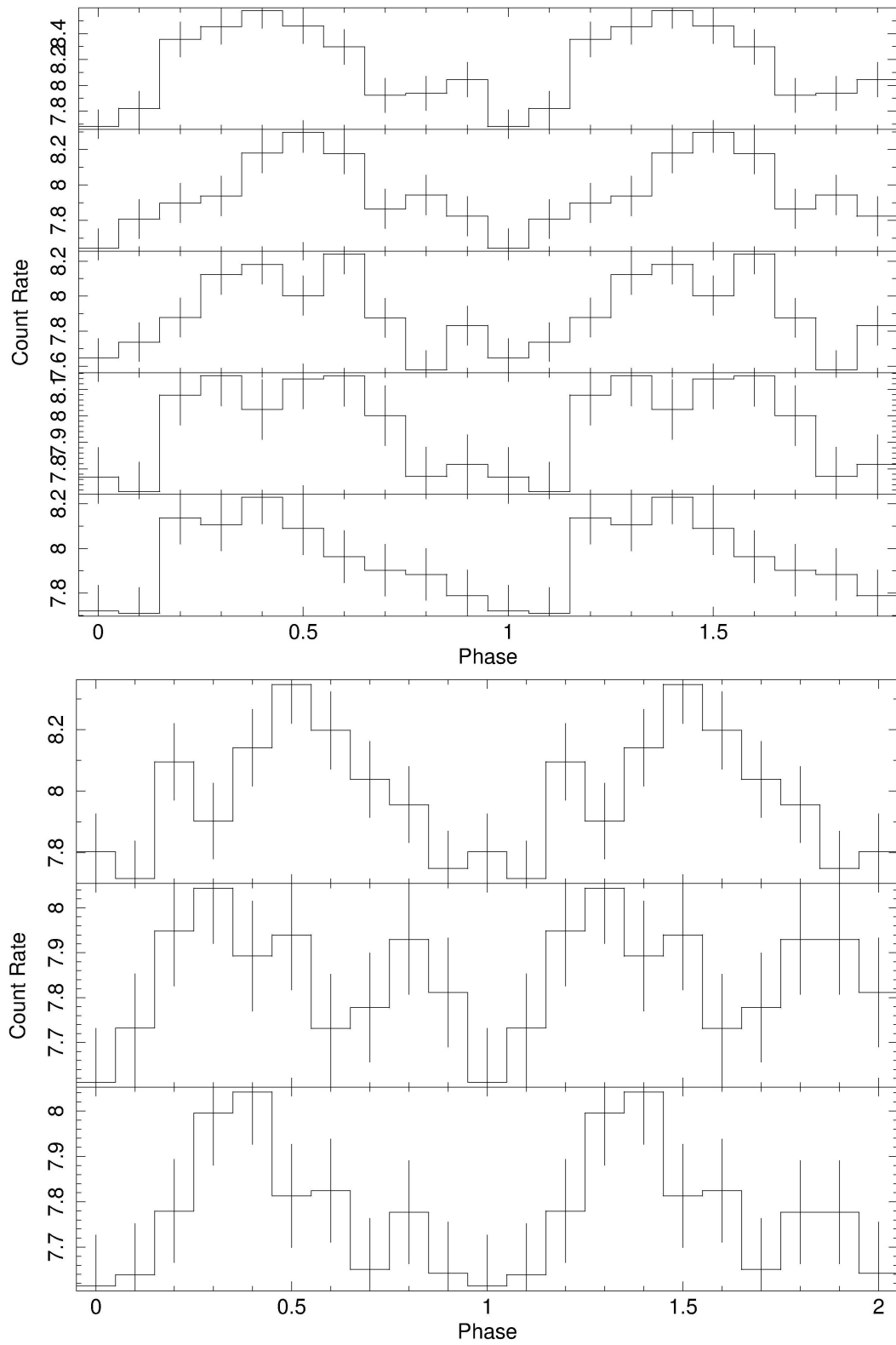


Figure 5.4. Pulse profiles of Swift J1834.9–0846

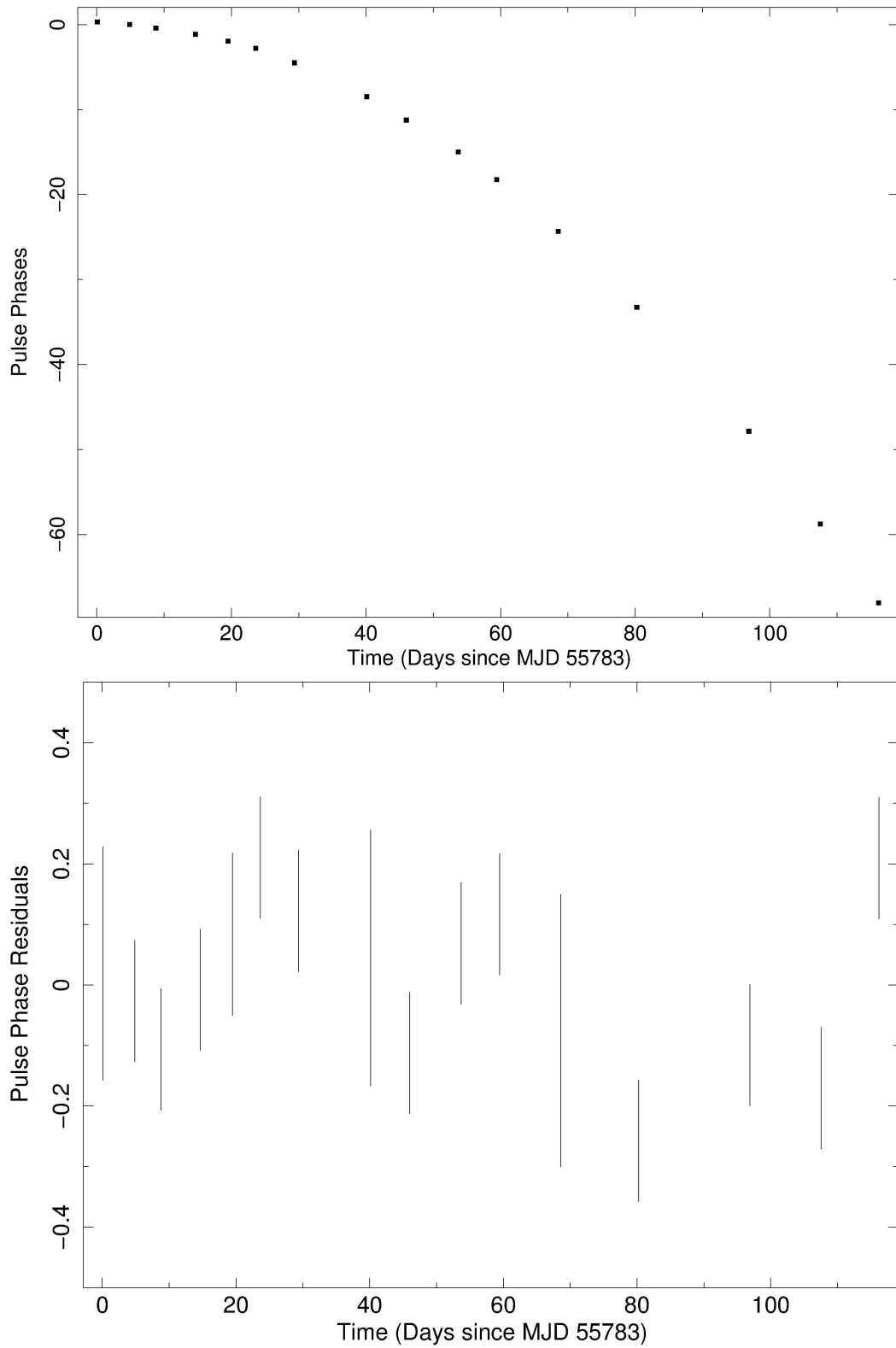


Figure 5.5. Pulse arrival times (top panel) and timing residuals (bottom panel) for Swift J1834.9-0846.

netic field of 1.51×10^{14} G at the surface the neutron star under the assumption of source is subject to magnetic dipole braking. And the second derivative of the frequency obtained from the model is $\ddot{\nu} = 3.2 \pm 1.3 \cdot 10^{-20}$ Hz/sec². Figure 5.1.3 represents pulse arrival times and the residuals of the timing solution.

5.2 Torque noise

Once the timing parameters for each magnetar are determined, we realized that residuals of the timing solution possess a noisy structure. It brings the idea that noise strength of these magnetars can be somehow correlated with another timing parameters as its shown among ordinary pulsars (Backer 2005; Dewey and Cordes 1989). Therefore, we started with extracting quadratic polynomial from our pulse arrival times for each source, hence obtained residuals of the timing solutions. Then, we estimated the associated timing noise strength from this residuals using Deeter polynomial estimator (Deeter and Boynton 1982).

Once the noise strengths for each magnetar are calculated, they are compared with other timing parameters. We found that noise strength is substantially correlated with spin down rate for these three SGRs, indicating that the faster its spinning down, the more noisy its rotation. Figure represents noise strengths versus absolute value of pulse frequency derivatives.

Preliminary interpretation of the correlation is that magnetic field stress on the crust can rupture pulsar's crust in micro scale, outcome of that event would be observed as torque noise in the pulse arrival times. However, in this thesis only three most recently discovered magnetars selected as subjects, we need to extend our work in order to obtain more statistically reliable association, hence a more thurstworthy comment on the correlation can be done.

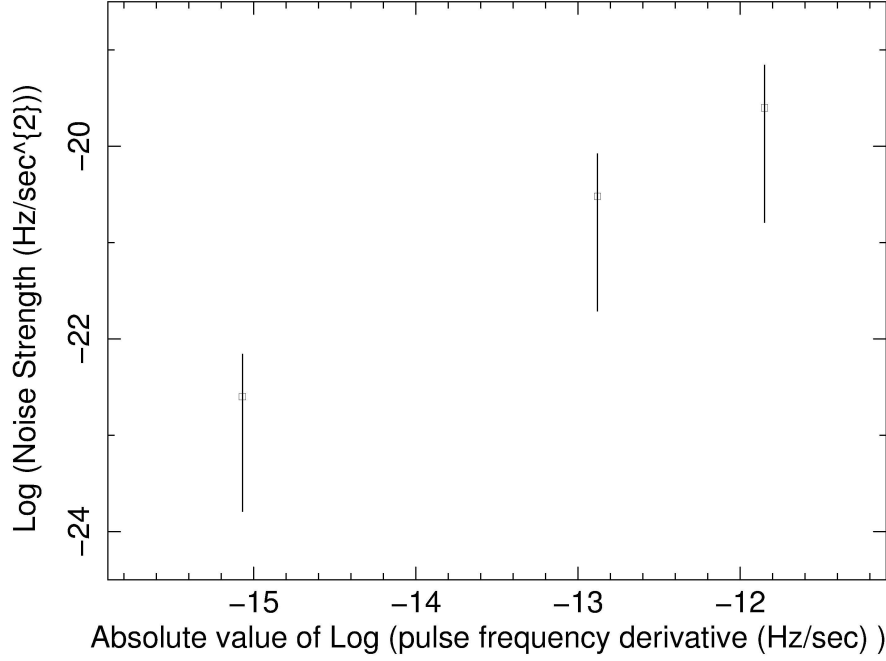


Figure 5.6. Noise strengths of three SGRs as a function of their pulse frequency derivatives.

5.3 Spectral analysis

Prior to the spectral data reduction, we chose observations suitable to carry out our analysis. As the RXTE has a large field of view, it also records emission from surrounding sources. Thus, making the data unable for performing spectral analysis. Therefore, results presented in this thesis will be from SWIFT (only PC mode), XMM-NEWTON and CHANDRA data. Spectral analyses are performed by modelling observational data by physical approximations in order to comprehend underlying physical mechanism that empowers magnetar emission. As it is mentioned in the previous chapters, SGR spectrum can be well defined by either a blackbody radiation or a powerlaw emission.

5.3.1 SGR J1833–0832

We analysed total 30 observations taken simulatenously by SWIFT-XRT, CHANDRA and XMM–Newton. Source events are chosen from the photons

fall within 20 pixels radius. Background events are selected from a region far away from the source because there exist other X-ray sources close to the magnetar SGR J1833–0832. We created spectrum for each observation and we represent the data with physical models using XSPEC package in FTOOLS. We tried to fit the data with blackbody or powerlaw models. Each model describes the spectrum very well (reduced χ^2 around 1). Adding second component to our model does not improve the quality of our fit statistically. So the results presented here are based on single component models. After we modeled each observation, we checked for the variability of the spectral parameters over time. Figure 5.7 represents the spectrum obtained by XMM-Newton data (obsID 0605852001).

In either case, even though flux levels differ, decay of the emission flux of the source keeps the same trend; the flux remains almost constant for 20 days and then starts to decrease until the source is undetectable. Assuming emission mechanism is a blackbody, we saw that corresponding emitting blackbody radius is shrinking gradually while other parameters are not significantly varying (Figure 5.8). If the emission mechanism is assumed to behave like power law, photon index of the emission is constant over the time till it reaches quiescent state indicating that source emission is not spectrally softening or hardening (Figure 5.8).

5.3.2 SWIFT J1822.3–1606

Spectral analysis of SWIFT J1822.3-1606 is carried out using 5 Swift-XRT observations taken in PC mode. For these observations, source events are extracted from 20 pixels radius circular region centering on image and annular region between 40-60 pixels are chosen for background events. Data is reprocessed, screened and filtered with prevalent options. Anchillary response file of the spectrum is obtained by "xrtmkarf" tool of Xselect. Once the spectrum from each observation is created, they are modeled by blackbody or power law models using XSPEC.

Both models can independently represent the data with statistically ac-

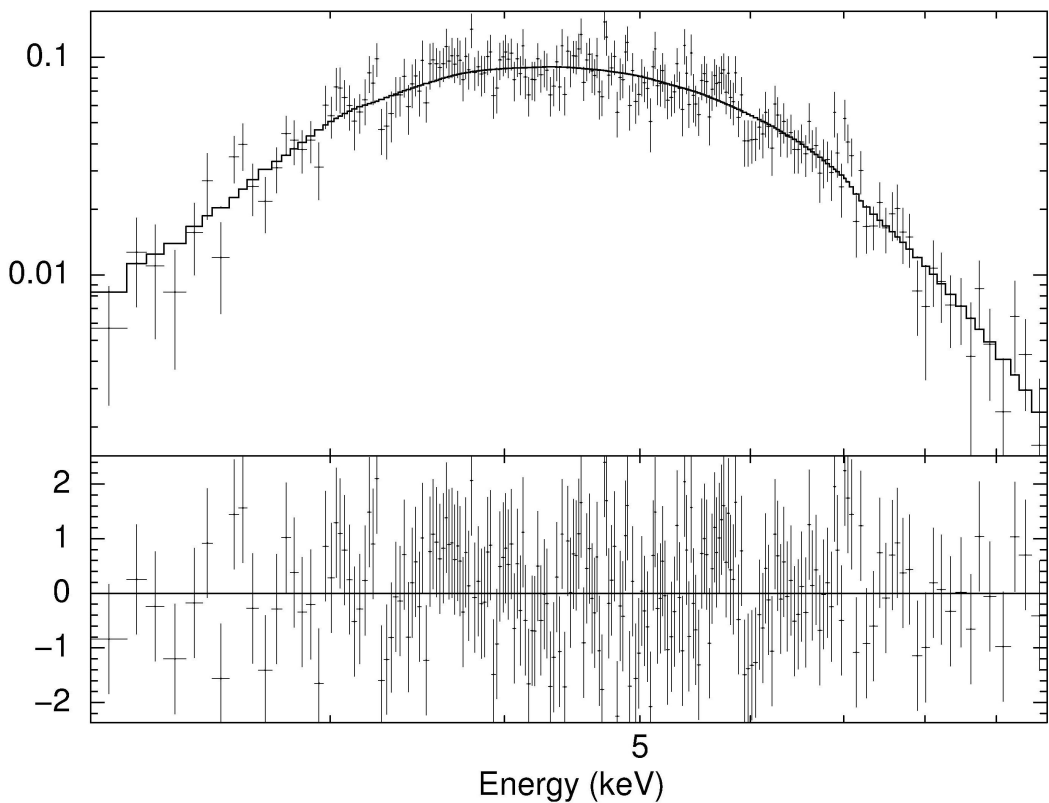
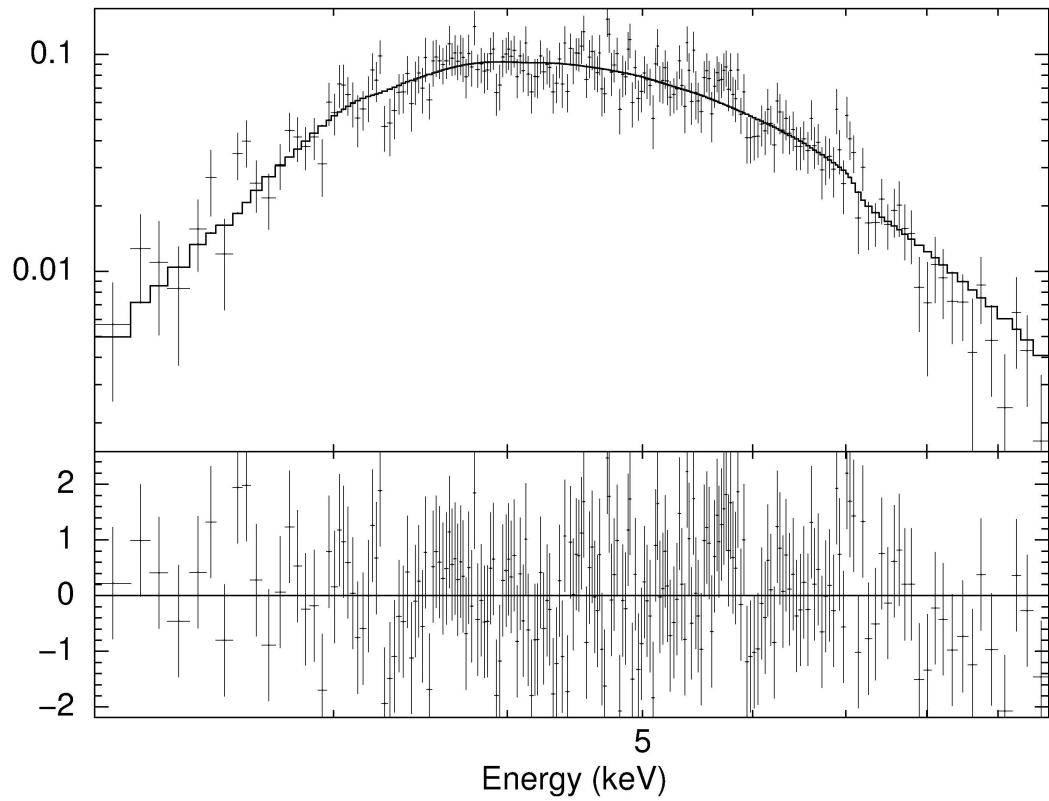


Figure 5.7. XMM-Newton Spectrum of SGR J1833–0832 with powerlaw model (top panel) and with blackbody model (bottom panel)

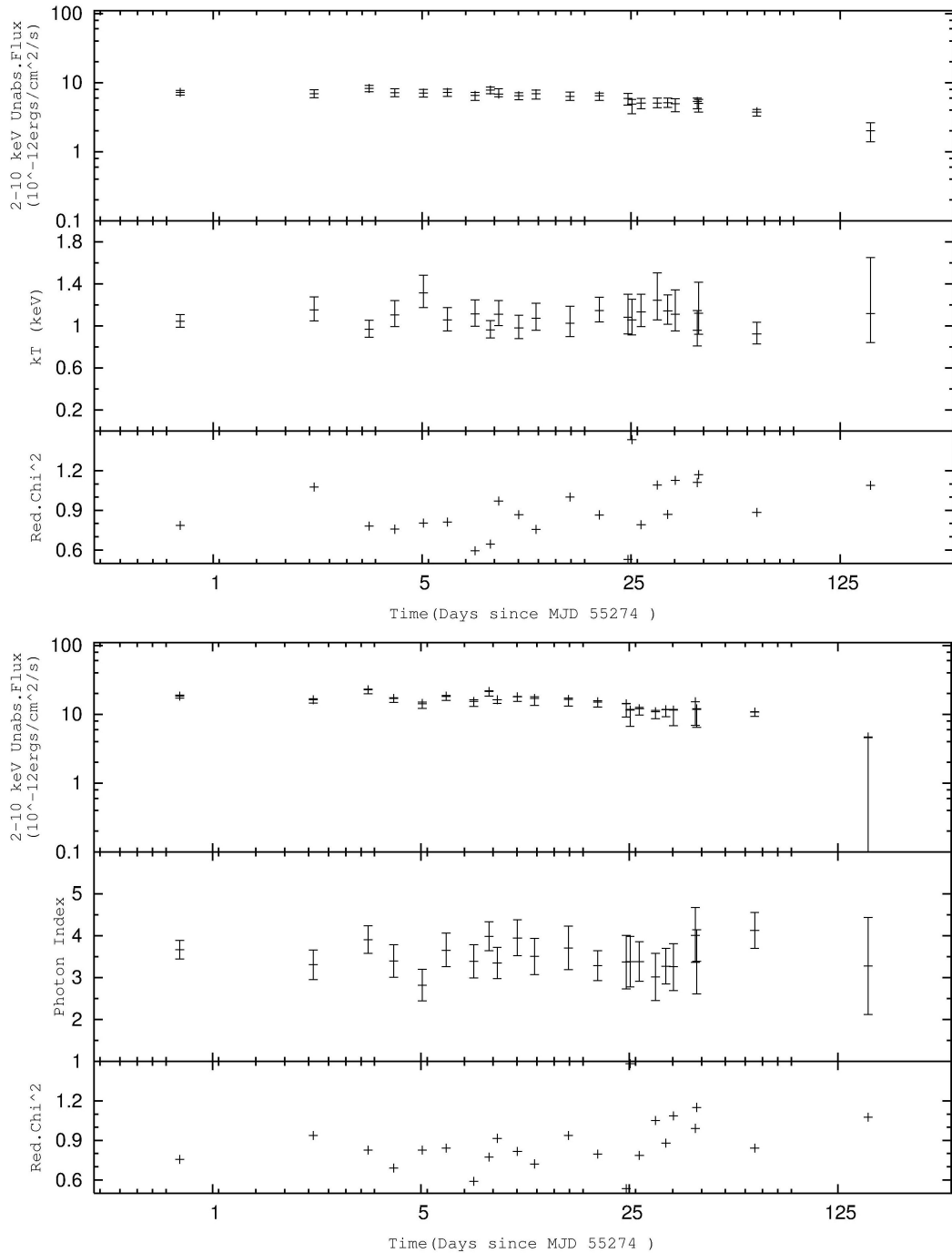


Figure 5.8. Variation of spectral parameters of SGR J1833–0832 with respect to time using blackbody emission model (top panel) and using power law model (bottom panel).

ceptable fits (see Figure 5.10). However, blackbody model fails to describe the data at relatively hard band through 7–10keV. Figure 5.9 illustrates a sample spectrum of the SWIFT J1822.3–1606 obtained from swift observation (obsID 00032033001) with blackbody and powerlaw models fits

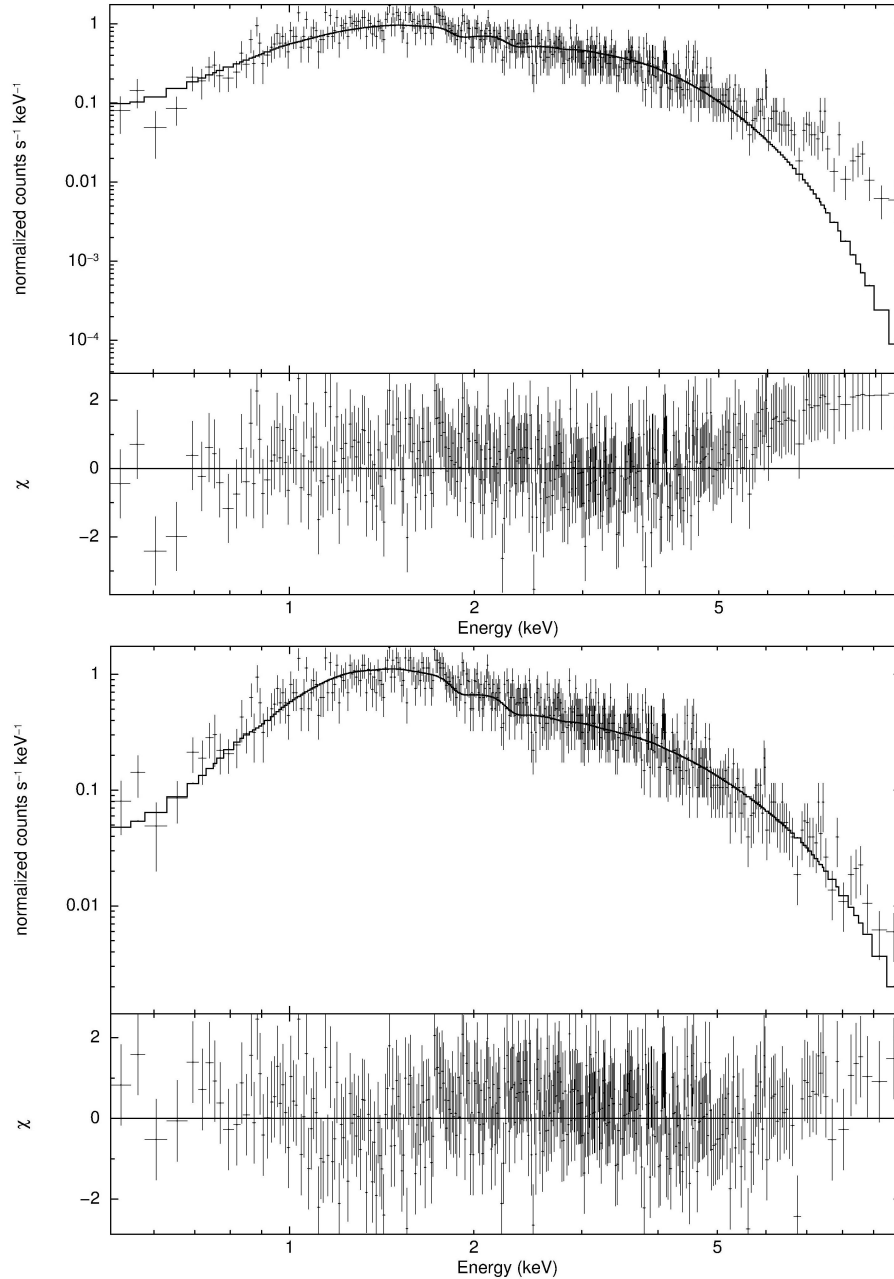


Figure 5.9. Swift spectrum of SWIFT J1822.3–1606 with blackbody model (top panel) and powerlaw model (bottom panel).

to the data. The spectral fit parameters for each observation is shown in the Figure 5.10. With blackbody model, temperature of the emission region is almost constant over time (kT around 0.6keV) and the radius of the emission region is shrinking as the flux of the source decays (Figure 5.10). However, in powerlaw model, photon index increased from 1.8 to 2.7 within 2 months, implying that emission of the source is softening with time (see Figure 5.10).

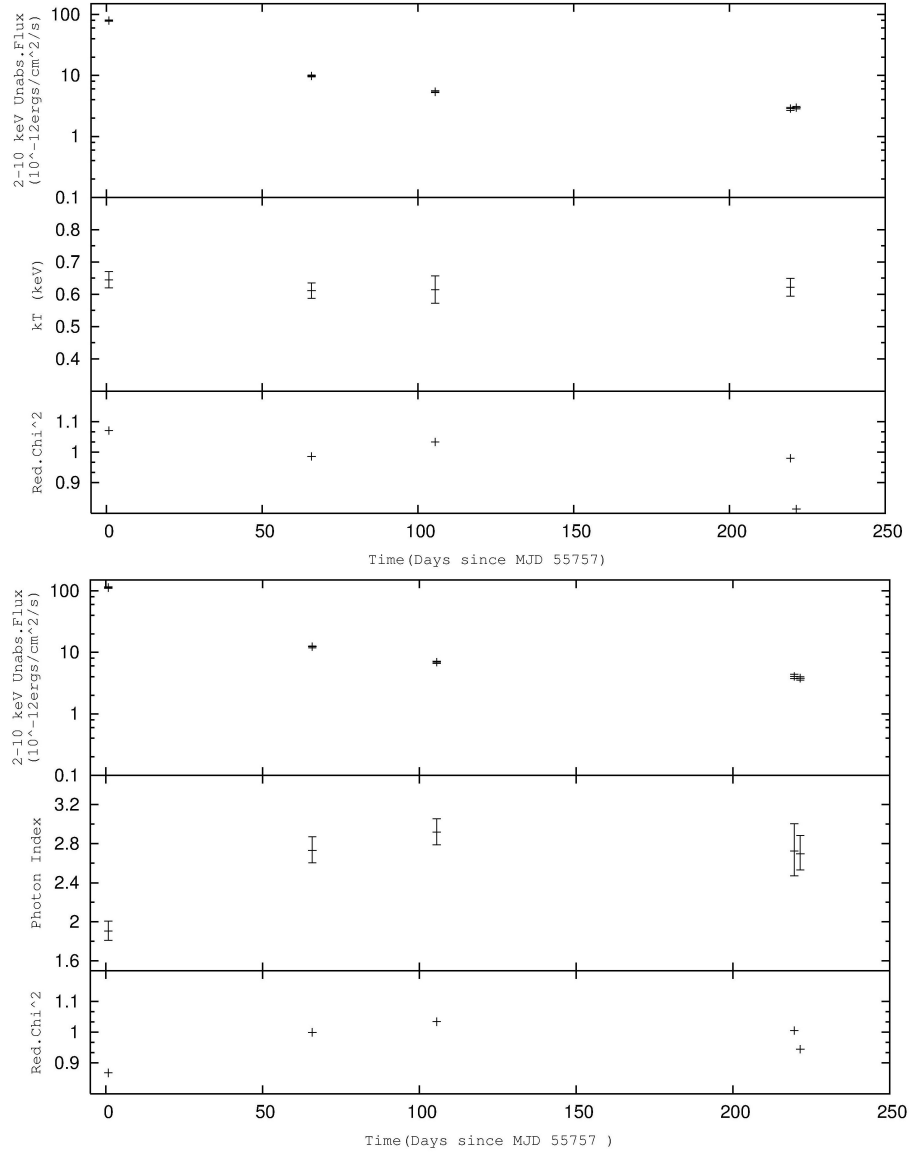


Figure 5.10. Variation of spectral parameters of SWIFT J1822.3–1606 with respect to time using blackbody emission model (top panel) and using power law model (bottom panel).

5.3.3 Swift J1834.9–0846

We performed spectral analysis for 1 XMM-Newton, 1 CHANDRA ACIS-S, and 3 SWIFT-XRT observations. Those three swift observations are combined into one because low counts in these observation does not allow to model the data. Filtering and screening options for all data are carried out by standard procedures. Source events are chosen from 20 pixels centering on the object and background events are chosen from a source free region far away from the object. For the XMM-Newton data, redistribution ma-

Table 5.3. Spectral parameters of Swift J1834.9–0846

Observation	Model	Nh	Photon Index	bbkT
Chandra	pl	15.3 ± 1.32	3.304 ± 0.2990	–
	bb	9.59 ± 0.863	–	1.061 ± 0.0614
XMM-Newton	pl	17.5 ± 1.38	4.357 ± 0.3051	–
	bb	9.3 ± 0.86	–	0.918 ± 0.0455
SWIFT-XRT (Combined)	pl	21.081 ± 3.77	2.728 ± 0.5539	–
	bb	13.71 ± 2.614	–	1.371 ± 0.1717

trices and ancillary reponses are created by RMFGEN and ARFGEN tasks of SAS software, while those of Chandra observations are extracted from spaceextract tool of CIAO software.

The resultant spectra are then modeled with either a blackbody or power-law emission both of which fits describe the data very well. The obtained parameters of spectral fits are shown in the Table 5.3.

Unlike SGR J1833–0832, lack of spectral observations does not allow to speculate long term variations of spectral parameters. However, pulsed count rate history of the source obtained from RXTE observations permits to illustrate time scale for flux decay of the Swift J1834.9–0846. The pulsed count rate history is generated by subtracting counts of pulse minima from the pulse maxima and acquired for the photons in 2-10 keV energy range (Figure 5.14).

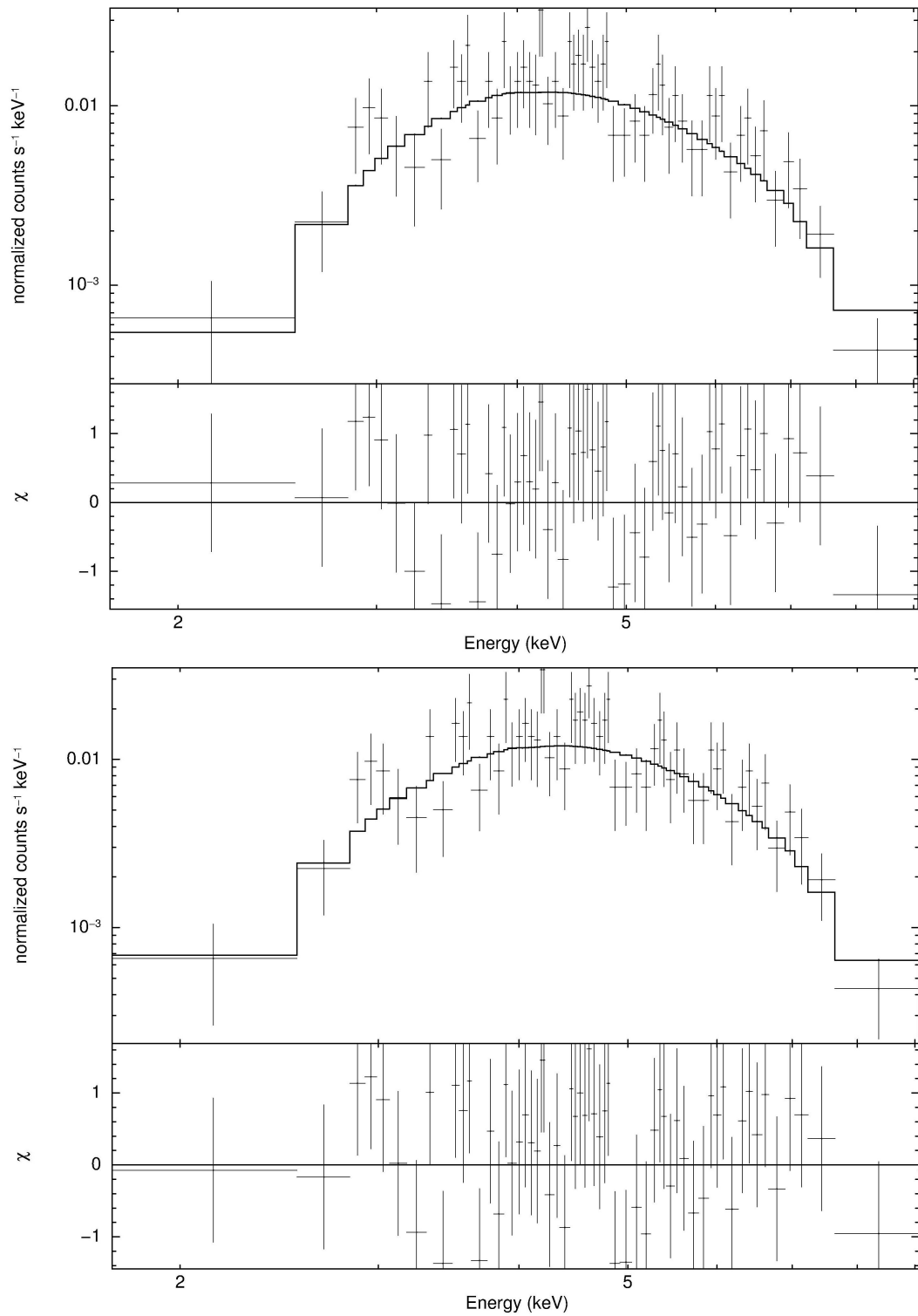


Figure 5.11. Swift spectrum of Swift J1834.9–0846 with powerlaw model (top panel) and blackbody emission model (bottom panel).

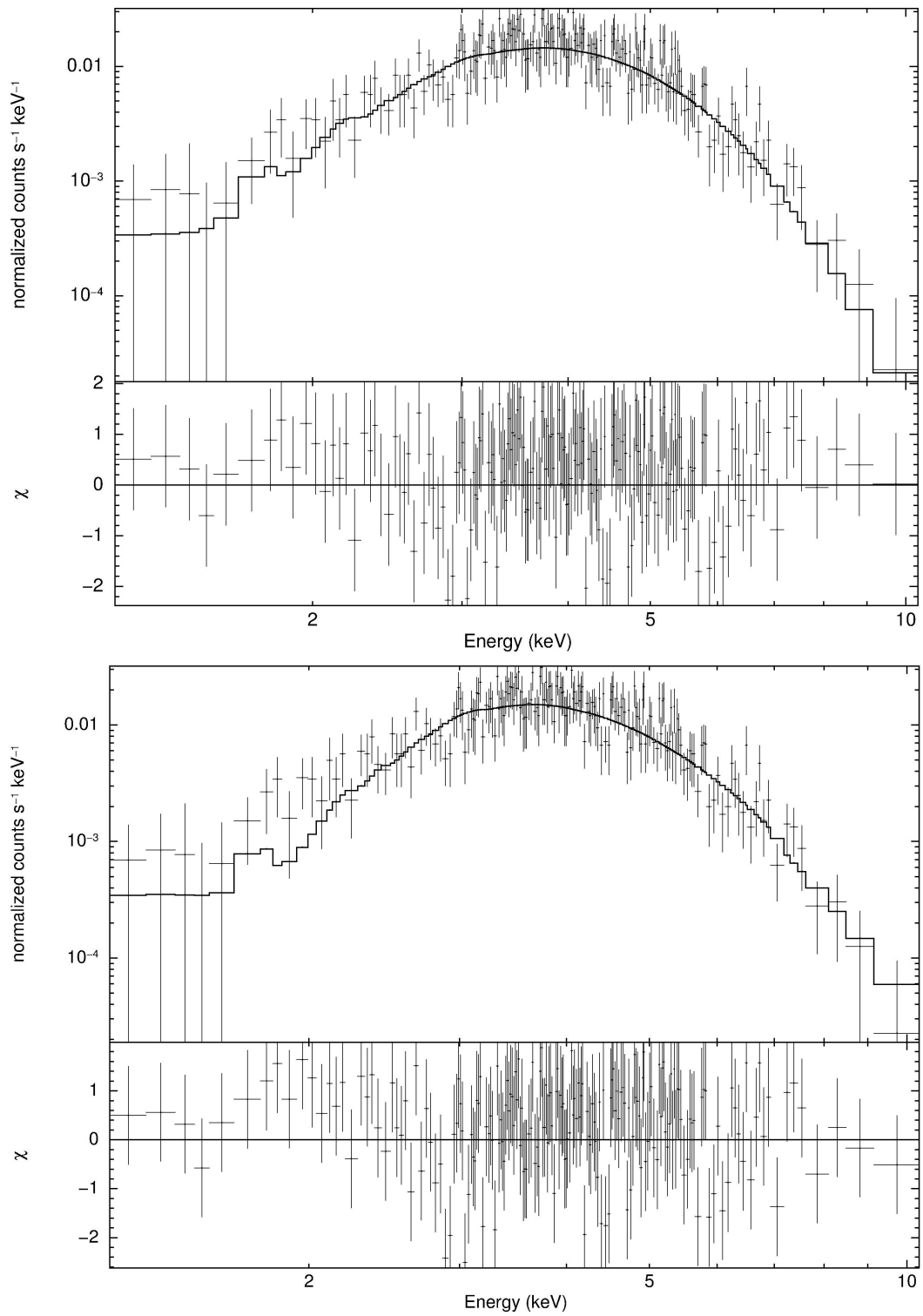


Figure 5.12. XMM-Newton spectrum of Swift J1834.9–0846 with blackbody emission model (top panel) and with powerlaw emission model (bottom panel).

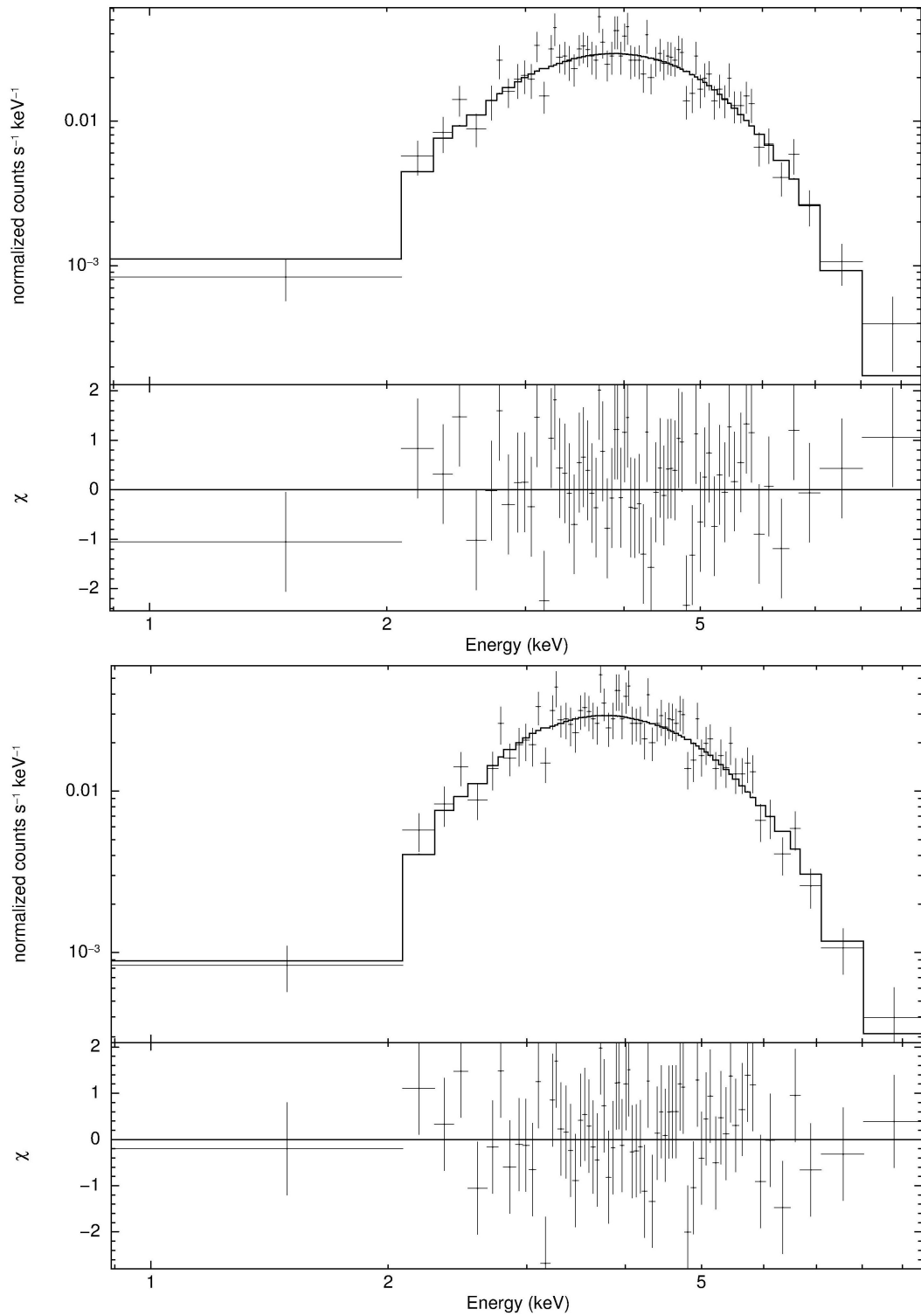


Figure 5.13. Chandra spectrum of Swift J1834.9–0846 with blackbody emission model (top panel) and powerlaw emission model (bottom panel).

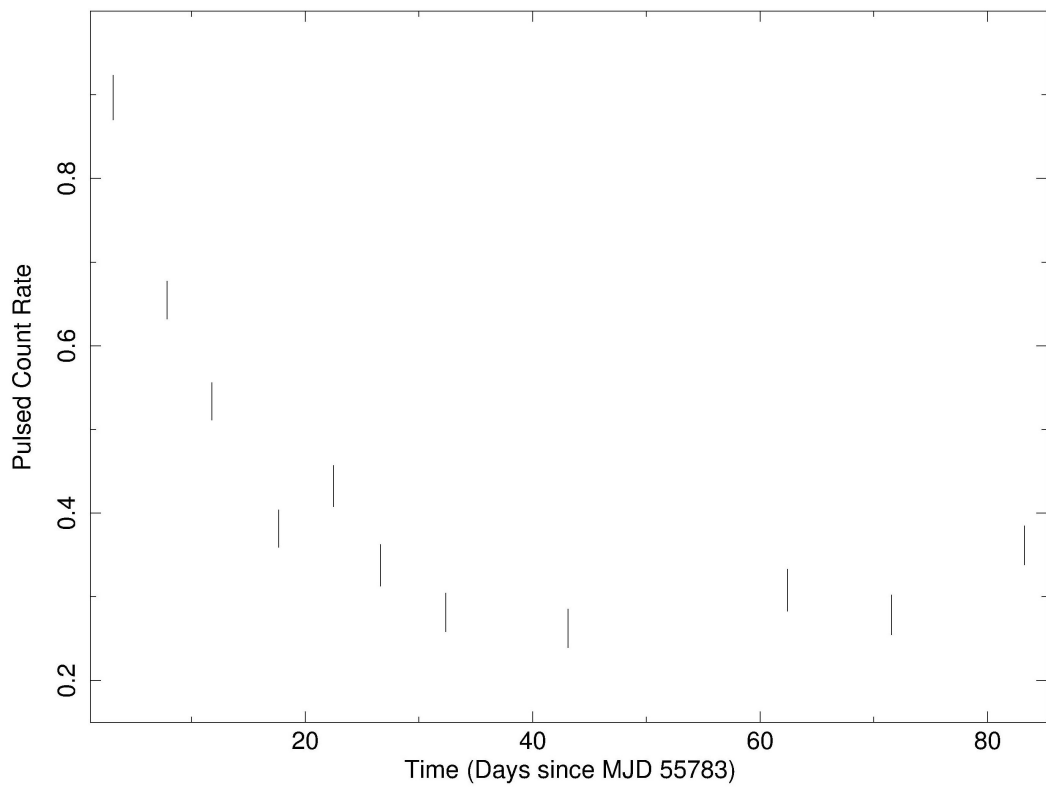


Figure 5.14. Pulsed count rate history of Swift J1834.9–0846

CHAPTER 6

CONCLUSION AND DISCUSSION

In this thesis, three most recently discovered Soft Gamma Repeaters are investigated in detail for their characteristic features. Spectral analysis of these neutron stars can aid to comprehend emission dynamics of SGRs and to test magnetar model. Combined Chandra, XMM-Newton, and Swift observations are used for that aim. In all the cases, obtained spectra can be described by either blackbody or a power law emission with the blackbody temperatures varying in between 0.8–1.4 keV and the photon index within 1.9–4.5. Time scales for flux decays are in orders of few 10 days, consistent with values that are put forward by magnetar model. However, main focus of this thesis is to gain an understanding on timing properties of SGRs. With this occasion, 81 RXTE measurements of SGR J1833–0832 for total exposure of 462 ks are analyzed to comprehend its timing characteristics. Resulting parameters revealed a coherent pulsation frequency of 0.13218076(8) Hz and frequency derivative of $-1.3529(9) \times 10^{-13}$ Hz/sec corresponding to a dipole field of 2.45×10^{14} G at the surface ensuring the magnetar nature of the object. Timing measurements of SWIFT J1822.3–1606 is carried out combining 34 RXTE and 38 Swift observations of total exposures 179 ks and 83 ks respectively. The obtained timing solution for SWIFT J1822.3–1606 yielded a spin frequency of 0.11851542(9) Hz and spin down rate of $8.4(3) \times 10^{-16}$ Hz/sec. Inferred dipole field strength from the timing parameters is 2.2×10^{13} G, implies that SWIFT J1822.3–1606 is the second weakest-dipole-fielded magnetar after SGR 0418+5729. As the deduced magnetic field is below the quan-

tum electrodynamic field strength of 4.4×10^{13} G, it can be suggested that true emission mechanism of magnetars may be linked with internal field rather than surface dipole field and it is necessary reconsider association of timing parameters with the magnetic field. Swift J1834.9-0846 is analyzed through the 17 RXTE observations with total exposure of 106 ks. Timing measurements for this source issued to a coherent signal at $\nu = 0.40285214(8)$ Hz with rather highly pulsed fraction, and the rotation period of Swift J1834.9-0846 indicates that the source is the second most rapidly-rotating magnetar among its class. The first frequency derivative of the SWIFT J1834.9-0846 is found to be $-1.462(2) \times 10^{-12}$ Hz/sec, and the deduced dipole field is in magnetar range, 1.51×10^{14} G. For all the cases in this three most recently discovered SGRs, residuals of the timing solutions stated above can be attributed to the second frequency derivative as well as a noise associated with torque. For the latter case, estimated torque noise strengths are found to be linked with their spin down rate suggesting that micro scale fractures on the magnetar's crust caused by magnetic field stress can account for the noise of the pulse arrival times. In the future, this work will be extended in order to have a more solid correlation and thereby substantial physical interpretation.

BIBLIOGRAPHY

- National Aeronautics and Space Administration (NASA). Swift technical handbook, appendix f. ftp://legacy.gsfc.nasa.gov/swift/nra_info/technical_appendix/, a.
- National Aeronautics and Space Administration (NASA). Xte technical appendix, appendix f. http://heasarc.gsfc.nasa.gov/docs/xte/appendix_f.html, b.
- National Aeronautics and Space Administration (NASA). The rossi x-ray timing explorer learning center, September 2011.
- M. A. Alpar. On Young Neutron Stars as Propellers and Accretors with Conventional Magnetic Fields. 554:1245–1254, June 2001. doi: 10.1086/321393.
- D. C. Backer. Timing Instabilities in Millisecond Pulsars. In F. A. Rasio and I. H. Stairs, editors, *Binary Radio Pulsars*, volume 328 of *Astronomical Society of the Pacific Conference Series*, page 385, July 2005.
- S. D. Barthelmy, T. Sakamoto, W. H. Baumgartner, J. R. Cummings, N. Gehrels, J. M. Gelbord, H. A. Krimm, C. B. Markwardt, D. M. Palmer, M. Stamatikos, J. Tueller, and T. N. Ukwatta. Swift-BAT refined analysis of the probable new Sgr 1833-0832. *GRB Coordinates Network*, 10528:1, 2010.
- M. Burgay, A. Possenti, P. Esposito, G. L. Israel, N. Rea, J. Sarkissian, A. Tiengo, R. Turolla, S. Zane, D. Gotz, L. Stella, and S. Mereghetti. Upper limit on the radio emission from the soft gamma-ray repeater SGR 1833-0832. *The Astronomer's Telegram*, 2515:1, March 2010.
- UK Swift Data Centre. Instruments on-board swift. <http://www.swift.ac.uk/about/instruments.php>.
- Smithsonian Astrophysical Observatory) Chandra X-ray Center (CXC). The chandra proposers' observatory guide. <http://cxc.harvard.edu/proposer/POG/html/index.html>, a.
- Smithsonian Astrophysical Observatory) Chandra X-ray Center (CXC). Pulsar bursts coming from beachball-sized structures. <http://www.nrao.edu/pr/2003/pulsaremission/>, b.
- P. Chatterjee, L. Hernquist, and R. Narayan. An Accretion Model for Anomalous X-Ray Pulsars. 534:373–379, May 2000. doi: 10.1086/308748.

- J. R. Cummings, D. Burrows, S. Campana, J. A. Kennea, H. A. Krimm, D. M. Palmer, T. Sakamoto, and S. Zan. Swift J1822.3-1606: A Probable New SGR in Ground Analysis of BAT Data. *The Astronomer's Telegram*, 3488:1, July 2011.
- J. E. Deeter and P. E. Boynton. Techniques for the estimation of red power spectra. I - Context and methodology. 261:337–350, October 1982. doi: 10.1086/160345.
- V. D'Elia, S. D. Barthelmy, W. H. Baumgartner, A. P. Beardmore, M. M. Chester, C. Guidorzi, S. T. Holland, N. P. M. Kuin, C. B. Markwardt, F. E. Marshall, A. Melandri, D. M. Palmer, C. J. Saxton, G. Stratta, C. A. Swenson, and T. N. Ukwatta. GRB 110807A: Swift detection of a burst or a possible new Sgr. *GRB Coordinates Network*, 12253:1, 2011.
- R. J. Dewey and J. M. Cordes. The scaling of radio pulsar timing noise with spin parameters. In H. Ögelman and E. P. J. van den Heuvel, editors, *Timing Neutron Stars*, page 119, 1989.
- R. C. Duncan and C. Thompson. Formation of very strongly magnetized neutron stars - Implications for gamma-ray bursts. 392:L9–L13, June 1992. doi: 10.1086/186413.
- Ü. Ertan, E. Göğüş, and M. A. Alpar. X-Ray and Infrared Enhancement of Anomalous X-Ray Pulsar 1E 2259+586. 640:435–440, March 2006. doi: 10.1086/500097.
- European Space Agency (ESA). Xmm-newton: A technical design. http://xmm.esac.esa.int/external/xmm_user_support/documentation/technical/Spacecraft/index.shtml, a.
- European Space Agency (ESA). Xmm-newton: A technical design. http://xmm.esac.esa.int/external/xmm_user_support/documentation/technical/Spacecraft/index.shtml, b.
- P. Esposito, G. L. Israel, R. Turolla, F. Mattana, A. Tiengo, A. Possenti, S. Zane, N. Rea, M. Burgay, D. Götz, S. Mereghetti, L. Stella, M. H. Wieringa, J. M. Sarkissian, T. Enoto, P. Romano, T. Sakamoto, Y. E. Nakagawa, K. Makishima, K. Nakazawa, H. Nishioka, and C. François-Martin. Long-term spectral and timing properties of the soft gamma-ray repeater SGR 1833-0832 and detection of extended X-ray emission around the radio pulsar PSR B1830-08. 416:205–215, September 2011. doi: 10.1111/j.1365-2966.2011.19022.x.
- D. Evans, R. Kiebasadel, J. Baros, T. Cline, U. Desai, B. Teegarden, G. Pizzichini, K. Hurley, M. Niel, G. Vedrenne, I. V. Estulin, and E. P. Mazets. Gamma-ray Burst 79-03-05. 3356:1, May 1979.
- G. G. Fahlman and P. C. Gregory. The Discovery of an X-Ray Pulsar in the SNR G109.1-1.0. In *Bulletin of the American Astronomical Society*, volume 13 of *Bulletin of the American Astronomical Society*, page 533, March 1981a.

- G. G. Fahlman and P. C. Gregory. An X-ray pulsar in SNR G109.1-1.0. 293:202–204, September 1981b. doi: 10.1038/293202a0.
- G. G. Fahlman and P. C. Gregory. The pulsation period and possible orbit of 1E2259 + 586. In J. Danziger and P. Gorenstein, editors, *Supernova Remnants and their X-ray Emission*, volume 101 of *IAU Symposium*, pages 445–453, 1983.
- F. P. Gavriil, V. M. Kaspi, and P. M. Woods. Anomalous X-ray pulsars: long-term monitoring and soft-gamma repeater like X-ray bursts. *Advances in Space Research*, 33:654–662, 2004. doi: 10.1016/j.asr.2003.07.023.
- E. Gogus. Archival Chandra Observations of SGR 1833-0832. *The Astronomer’s Telegram*, 2495:1, March 2010.
- E. Gogus and C. Kouveliotou. RXTE Discovery of the Spin Period of Swift J1834.9-0846. *The Astronomer’s Telegram*, 3542:1, August 2011.
- E. Gogus, T. Strohmayer, C. Kouveliotou, and P. Woods. Discovery of the spin period of Sgr 1833-0832. *GRB Coordinates Network*, 10534:1, 2010.
- E. Gogus, C. Kouveliotou, O. Kargaltsev, and G. Pavlov. Swift J1834.9-0846: Precise X-ray Position and the Confirmation of its Spin Period. *The Astronomer’s Telegram*, 3576:1, August 2011a.
- E. Gogus, C. Kouveliotou, and T. Strohmayer. RXTE Detection of the Spin Period of Swift J1822.3-1606. *The Astronomer’s Telegram*, 3491:1, July 2011b.
- E. Gogus, C. Kouveliotou, and T. Strohmayer. Swift J1822.3-1606. *GRB Coordinates Network*, 12167:1, 2011c.
- S. V. Golenetskii, V. N. Ilinskii, and E. P. Mazets. Recurrent bursts in GBS0526 - 66, the source of the 5 March 1979 gamma-ray burst. 307: 41–43, January 1984. doi: 10.1038/307041a0.
- E. Göğüş, G. Cusumano, A. J. Levan, C. Kouveliotou, T. Sakamoto, S. D. Barthelmy, S. Campana, Y. Kaneko, B. W. Stappers, A. de Ugarte Postigo, T. Strohmayer, D. M. Palmer, J. Gelbord, D. N. Burrows, A. J. van der Horst, T. Muñoz-Darias, N. Gehrels, J. W. T. Hessels, A. P. Kamble, S. Wachter, K. Wiersema, R. A. M. J. Wijers, and P. M. Woods. Discovery of a New Soft Gamma Repeater, SGR J1833-0832. 718:331–339, July 2010. doi: 10.1088/0004-637X/718/1/331.
- S. Guiriec, C. Kouveliotou, and A. J. van der Horst. Fermi GBM detection of a SGR-like burst. *GRB Coordinates Network*, 12255:1, 2011.
- G. L. Israel, S. Mereghetti, and L. Stella. The discovery of 8.7 second pulsations from the ultrasoft X-ray source 4U 0142+61. 433:L25–L28, September 1994. doi: 10.1086/187539.
- F. Jansen, D. Lumb, B. Altieri, J. Clavel, M. Ehle, C. Erd, C. Gabriel, M. Guainazzi, P. Gondoin, R. Much, R. Munoz, M. Santos, N. Schartel, D. Texier, and G. Vacanti. XMM-Newton observatory. I. The spacecraft

- and operations. 365:L1–L6, January 2001. doi: 10.1051/0004-6361:20000036.
- O. Kargaltsev, E. Gogus, C. Kouveliotou, and G. Pavlov. Unusually strong X-ray pulsations from Swift J1834.9-0846. *The Astronomer's Telegram*, 3600:1, August 2011.
- Kargaltsev, O. and Kouveliotou, C. and Pavlov, G. G. and Göğüş, E. and Lin, L. and Wachter, S. and Griffith, R. L. and Kaneko, Y. and Younes, G. X-Ray Observations of the New Unusual Magnetar Swift J1834.9-0846. 748:26, mar 2012. doi: {10.1088/0004-637X/748/1/26}.
- C. Kouveliotou. A Review of Soft Gamma Repeaters (SGRs). In E. P. van den Heuvel, L. Kaper, E. Rol, and R. A. M. J. Wijers, editors, *From X-ray Binaries to Gamma-Ray Bursts: Jan van Paradijs Memorial Symposium*, volume 308 of *Astronomical Society of the Pacific Conference Series*, page 413, 2003.
- C. Kouveliotou, S. Dieters, T. Strohmayer, J. van Paradijs, G. J. Fishman, C. A. Meegan, K. Hurley, J. Kommers, I. Smith, D. Frail, and T. Murakami. An X-ray pulsar with a superstrong magnetic field in the soft γ -ray repeater SGR1806 - 20. 393:235–237, May 1998. doi: 10.1038/30410.
- L. Kuiper and W. Hermsen. The spin-down of Swift J1834.9-0846: confirmation as magnetar. *The Astronomer's Telegram*, 3577:1, August 2011.
- J. G. Laros, E. E. Fenimore, M. M. Fikani, R. W. Klebesadel, and C. Barat. The soft gamma-ray burst GB790107. 322:152, July 1986. doi: 10.1038/322152a0.
- M. A. Livingstone, P. Scholz, V. M. Kaspi, C.-Y. Ng, and F. P. Gavriil. The Spin-down of Swift J1822.3-1606: A New Galactic Magnetar. 743:L38, December 2011. doi: 10.1088/2041-8205/743/2/L38.
- F. E. Marshall and J. M. Gelbord. SGR 1833-0832: Swift/UVOT upper limits. *GRB Coordinates Network*, 10540:1, 2010.
- E. P. Mazets, S. V. Golenetskii, V. N. Il'Inskii, V. N. Panov, R. L. Aptekar', Y. A. Gur'yan, I. A. Sokolov, Z. Y. Sokolova, and T. V. Kharitonova. A flaring x-ray pulsar in Dorado. *Soviet Astronomy Letters*, 5:163, April 1979.
- S. Mereghetti and L. Stella. The very low mass X-ray binary pulsars: A new class of sources? 442:L17–L20, March 1995. doi: 10.1086/187805.
- A. S. Moskvitin, V. V. Sokolov, and R. I. Uklein. GRB 110807A: SAO RAS observations. *GRB Coordinates Network*, 12254:1, 2011.
- National Radio Astronomy Observatory). The chandra proposers' observatory guide. <http://cxc.harvard.edu/proposer/POG/html/chap1.html>.

- C. Pagani, A. P. Beardmore, and J. A. Kennea. Swift J1822.3-1606: Enhanced Swift-XRT position. *The Astronomer's Telegram*, 3493:1, July 2011.
- D. Palmer and J. M. Gelbord. SGR 1833-0832 is pulsed at 7.56 seconds. *GRB Coordinates Network*, 10537:1, 2010.
- R. Perna, J. S. Heyl, L. E. Hernquist, A. M. Juett, and D. Chakrabarty. Anomalous X-Ray Pulsars and Soft Gamma-Ray Repeaters: Spectral Fits and the Magnetar Model. 557:18–23, August 2001. doi: 10.1086/321569.
- N. Rea, R. P. Mignani, G. L. Israel, and P. Esposi. Optical observations of Swift J1822.3-1606 with the 10.4m Gran Telescopio Canarias. *The Astronomer's Telegram*, 3515:1, July 2011.
- N. Rea, G. L. Israel, P. Esposito, J. A. Pons, A. Camero-Arranz, R. P. Mignani, R. Turolla, S. Zane, M. Burgay, A. Possenti, S. Campana, T. Enoto, N. Gehrels, E. Göğüş, D. Götz, C. Kouveliotou, K. Makishima, S. Mereghetti, S. R. Oates, D. M. Palmer, R. Perna, L. Stella, and A. Tiengo. A New Low Magnetic Field Magnetar: The 2011 Outburst of Swift J1822.3-1606. 754:27, July 2012. doi: 10.1088/0004-637X/754/1/27.
- P. Scholz, C.-Y. Ng, M. A. Livingstone, V. M. Kaspi, A. Cumming, and R. Archibald. Swift J1822.3-1606: Post-outburst evolution of a nearby magnetar. *ArXiv e-prints*, April 2012.
- F. D. Seward, P. A. Charles, and A. P. Smale. A 6 second periodic X-ray source in Carina. 305:814–816, June 1986. doi: 10.1086/164294.
- C. Thompson and R. C. Duncan. The soft gamma repeaters as very strongly magnetized neutron stars - I. Radiative mechanism for outbursts. 275:255–300, July 1995.
- C. Thompson and R. C. Duncan. The Soft Gamma Repeaters as Very Strongly Magnetized Neutron Stars. II. Quiescent Neutrino, X-Ray, and Alfvén Wave Emission. 473:322, December 1996. doi: 10.1086/178147.
- J. van Paradijs, R. E. Taam, and E. P. J. van den Heuvel. On the nature of the 'anomalous' 6-s X-ray pulsars. 299:L41, July 1995.
- K.-P. Wenzel, editor. *Report on the Activities of the Research and Scientific Support Department*, volume 1268 of *ESA Special Publication*, March 2003.
- P. M. Woods and C. Thompson. *Soft gamma repeaters and anomalous X-ray pulsars: magnetar candidates*, pages 547–586. April 2006.
- Peter M. Woods and C. Thompson. *Soft gamma repeaters and anomalous x-ray pulsars: Magnetar candidates*. 2004.

G. Younes, C. Kouveliotou, O. Kargaltsev, G. G. Pavlov, E. Göğüş, and S. Wachter. XMM-Newton View of Swift J1834.9-0846 and Its Magnetar Wind Nebula. 757:39, September 2012. doi: 10.1088/0004-637X/757/1/39.

APPENDIX A

APPENDIX

In the following tables, SAT is the satellite; Date is in YYYY-MM-DD format, Exposure Time (EXP) is in seconds.

Table A.1. Journal of RXTE observations of SWIFT J1822.3-1606

Observation ID	Date	EXP	Observation ID	Date	EXP
96048-01-01-00	2011-07-14	600	96048-02-04-02	2011-08-11	3547
96048-02-01-00	2011-07-16	6542	96048-02-05-02	2011-08-12	3354
96048-02-01-05	2011-07-18	1653	96048-02-05-00	2011-08-15	5932
96048-02-01-01	2011-07-19	4998	96048-02-05-01	2011-08-16	5928
96048-02-01-02	2011-07-20	4894	96048-02-06-00	2011-08-21	6560
96048-02-01-04	2011-07-21	3230	96048-02-07-00	2011-08-26	6885
96048-02-01-03	2011-07-21	6011	96048-02-08-00	2011-09-06	5991
96048-02-02-00	2011-07-22	6061	96048-02-10-00	2011-09-16	6688
96048-02-02-01	2011-07-23	6755	96048-02-10-01	2011-09-22	5583
96048-02-02-02	2011-07-25	2946	96048-02-09-00	2011-09-25	6277
96048-02-02-03	2011-07-27	3043	96048-02-11-00	2011-10-01	7073
96048-02-03-00	2011-07-29	6761	96048-02-12-00	2011-10-08	5874
96048-02-03-01	2011-08-01	6869	96048-02-13-00	2011-10-15	5667
96048-02-03-02	2011-08-04	1951	96048-02-14-00	2011-10-29	6767
96048-02-03-04	2011-08-04	1718	96048-02-16-00	2011-11-13	5950
96048-02-04-00	2011-08-07	6675	96048-02-17-00	2011-11-20	5994
96048-02-04-01	2011-08-09	6298	96048-02-15-00	2011-11-28	6685

Table A.2. Journal of RXTE observations of SGR J1833-0832

Observation ID	Date	EXP	Observation ID	Date	EXP
95048-03-01-10	2010-03-19	1331	95048-03-13-00	2010-06-13	6491
95048-03-01-00	2010-03-21	10443	95048-03-13-01	2010-06-17	6770
95048-03-01-01	2010-03-21	6892	95048-03-14-00	2010-06-22	5708
95048-03-01-02	2010-03-21	13396	95048-03-15-00	2010-06-25	6265
95048-03-01-04	2010-03-23	11936	95048-03-15-01	2010-06-28	6780
95048-03-01-03	2010-03-23	9719	95048-03-15-02	2010-07-01	232
95048-03-01-05	2010-03-24	3445	95048-03-16-00	2010-07-02	5634
95048-03-01-07	2010-03-24	3056	95048-03-16-01	2010-07-05	5972
95048-03-01-08	2010-03-25	6723	95048-03-16-02	2010-07-08	6110
95048-03-02-00	2010-03-26	6451	95048-03-17-00	2010-07-14	5577
95048-03-02-01	2010-03-27	6562	95048-03-18-00	2010-07-19	6183
95048-03-02-02	2010-03-28	5412	95048-03-18-01	2010-07-22	4939
95048-03-02-03	2010-03-29	5960	95048-03-19-00	2010-07-26	6752
95048-03-02-04	2010-03-30	5616	95048-03-19-01	2010-07-29	6759
95048-03-02-05	2010-04-01	2641	95048-03-20-00	2010-08-02	5998
95048-03-02-06	2010-04-01	3231	95048-03-21-00	2010-08-08	6730
95048-03-03-00	2010-04-02	6804	95048-03-21-01	2010-08-11	6775
95048-03-03-01	2010-04-03	3367	95048-03-22-00	2010-08-14	5948
95048-03-03-06	2010-04-03	3378	95048-03-22-01	2010-08-17	5611
95048-03-03-02	2010-04-03	6774	95048-03-23-00	2010-08-21	5447
95048-03-03-05	2010-04-06	3428	95048-03-23-01	2010-08-23	6614
95048-03-04-00	2010-04-09	5810	95048-03-23-02	2010-08-26	5291
95048-03-04-01	2010-04-13	5116	95048-03-24-00	2010-08-31	5275
95048-03-05-00	2010-04-18	6824	95048-03-25-00	2010-09-03	6393
95048-03-06-00	2010-04-23	6949	95048-03-25-01	2010-09-07	6422
95048-03-06-01	2010-04-26	2861	95048-03-26-00	2010-09-10	6064
95048-03-06-02	2010-04-26	3360	95048-03-26-01	2010-09-13	5162
95048-03-07-00	2010-04-30	6892	95048-03-27-00	2010-09-17	6565
95048-03-07-01	2010-05-03	3313	95048-03-27-01	2010-09-21	6136
95048-03-07-03	2010-05-03	3363	95048-03-28-00	2010-09-24	6033
95048-03-07-02	2010-05-06	6773	95048-03-29-00	2010-10-03	5931
95048-03-08-01	2010-05-12	5714	95048-03-30-00	2010-10-11	6828
95048-03-09-00	2010-05-15	5755	95048-03-31-00	2010-10-17	5687
95048-03-09-01	2010-05-18	5980	95048-03-32-00	2010-10-30	5236
95048-03-10-00	2010-05-24	6355	95048-03-33-00	2010-11-07	1804
95048-03-11-00	2010-05-28	5719	95048-03-33-01	2010-11-08	2240
95048-03-11-01	2010-05-31	5378	95048-03-33-02	2010-11-08	1780
95048-03-11-02	2010-06-03	5906	95048-03-34-00	2010-11-14	6739
95048-03-12-00	2010-06-07	5359	95048-03-35-00	2010-11-23	6143
95048-03-12-01	2010-06-10	6498	95048-03-36-00	2010-11-29	6497
			95048-03-37-00	2010-12-03	6020

Table A.3. Journal of RXTE observations of SWIFT J1834.9-0846

Observation ID	Date	EXP
96434-01-01-00	2011-08-09	3480
96434-01-02-00	2011-08-09	10173
96434-01-03-00	2011-08-14	6881
96434-01-03-01	2011-08-18	6905
96434-01-04-00	2011-08-24	6729
96434-01-05-00	2011-08-29	6210
96434-01-06-00	2011-09-02	5635
96434-01-06-01	2011-09-08	5656
96434-01-08-00	2011-09-19	6249
96434-01-07-00	2011-09-24	6289
96434-01-09-00	2011-10-02	5932
96434-01-10-00	2011-10-08	5687
96434-01-11-00	2011-10-17	5835
96434-01-12-00	2011-10-29	6057
96434-01-14-00	2011-11-14	6209
96434-01-13-00	2011-11-25	6032
96434-01-15-00	2011-12-04	6441

Table A.4. Journal of SWIFT observations of SWIFT J1822.3-1606 (windowed timing mode)

Observation ID	Date	EXP
Windowed Timing mode		
00032033002	2011-07-16	1999.605
00032033003	2011-07-17	1999.62
00032033005	2011-07-19	478.888
00032033006	2011-07-20	1808.27
00032033007	2011-07-21	1634.213
00032033008	2011-07-23	2248.505
00032033009	2011-07-24	1704.066
00032033010	2011-07-27	2119.22
00032033011	2011-07-28	2074.209
00032033012	2011-07-29	2144.529
00032033013	2011-07-30	2098.949
00032051001	2011-08-04	1831.714
00032051002	2011-08-06	1729.126
00032051003	2011-08-07	2289.06
00032051004	2011-08-08	2259.161
00032051005	2011-08-13	2234.057
00032051006	2011-08-14	2154.269
00032051007	2011-08-15	2284.225
00032051008	2011-08-16	2228.883
00032051009	2011-08-17	2174.061
00032033014	2011-08-20	134.617
00032033015	2011-08-27	2918.778
00032033016	2011-09-03	2389.053
00032033018	2011-09-20	1502.542
00032033019	2011-09-25	2308.387
00032033021	2011-10-07	4233.539
00032033022	2011-10-15	3469.908
00032033023	2011-10-22	2253.518
00032033026	2012-02-20	10251.90
00032033029	2012-02-25	6984.764
00032033030	2012-02-28	7011.73
Photon Timing mode		
32033001	2011-07-15	1591.993
32033017	2011-09-18	4963.795
32033024	2011-10-28	10274.354
32033025	2012-02-19	6245.489
32033027	2012-02-21	11013.9

Table A.5. Journal of SWIFT observations for SGR1833-0832 (Photon Counting mode)

Observation ID	Date	EXP
00416485000	2010-03-19	29434.1750
00416485001	2010-03-21	10825.9910
00416485002	2010-03-21	9978.34200
00416485003	2010-03-22	13420.8180
00416485004	2010-03-23	12980.8570
00416485005	2010-03-24	10341.6510
00416485006	2010-03-25	9886.29000
00416485007	2010-03-26	10068.7610
00416485008	2010-03-27	9904.64600
00416485009	2010-03-27	10976.9120
00416485010	2010-03-29	9557.07000
00416485011	2010-03-31	7956.45700
00416485012	2010-04-03	10069.2850
00416485013	2010-04-07	10144.1800
00416485014	2010-04-12	5157.68300
00416485015	2010-04-13	4076.83700
00416485016	2010-04-14	9501.06400
00416485017	2010-04-18	8892.33800
00416485018	2010-04-21	10358.4330
00416485019	2010-04-23	7634.05300
00416485020	2010-04-29	5598.94300
00416485021	2010-04-30	4382.06900
00416485022	2010-05-23	18171.8960
00416485023	2010-08-24	5382.93000
00416485024	2010-08-25	2251.98600
00416485025	2010-08-26	9961.51800
00416485026	2010-08-27	2544.19100

Table A.6. Journal of other observations.

SAT	Observation ID	Date	EXP	
SWIFT	SWIFT J1834.9-0846	00458907014	2011-09-02	2072.933
SWIFT	SWIFT J1834.9-0846	00458907015	2011-09-05	1852.885
SWIFT	SWIFT J1834.9-0846	00458907016	2011-09-10	2020.848
XMM-Newton	SWIFT J1834.9-0846	0679380201	2011-09-17	28917
XMM-Newton	SGR J1833-0832	0605852101	2010-04-13	18916
XMM-Newton	SGR J1833-0832	0605851901	2010-03-23	23194
XMM-Newton	SGR J1833-0832	0605852001	2010-04-02	22913
Chandra	SGR J1833-0832	11114	2010-03-23	33550
Chandra	SWIFT J1834.9-0846	14329	2011-08-22	14350